Advances in Understanding Clouds from ISCCP

William B. Rossow* and Robert A. Schiffer+

ABSTRACT

This progress report on the International Satellite Cloud Climatology Project (ISCCP) describes changes made to produce new cloud data products (D data), examines the evidence that these changes are improvements over the previous version (C data), summarizes some results, and discusses plans for the ISCCP through 2005. By late 1999 all datasets will be available for the period from July 1983 through December 1997. The most significant changes in the new D-series cloud datasets are 1) revised radiance calibrations to remove spurious changes in the long-term record, 2) increased cirrus detection sensitivity over land, 3) increased low-level cloud detection sensitivity in polar regions, 4) reduced biases in cirrus cloud properties using an ice crystal microphysics model in place of a liquid droplet microphysics model, and 5) increased detail about the variations of cloud properties. The ISCCP calibrations are now the most complete and self-consistent set of calibrations available for all the weather satellite imaging radiometers: total relative uncertainties in the radiance calibrations are estimated to be 5% for visible and 2% for infrared; absolute uncertainties are < 10% and < 3%, respectively. Biases in (detectable) cloud amounts have been reduced to 0.05, except in the summertime polar regions where the bias may still be ~ 0.10. Biases in cloud-top temperatures have been reduced to 2 K for lower-level clouds and 4 K for optically thin, upper-level clouds, except when they occur over lower-level clouds. Using liquid and ice microphysics models reduces the biases in cloud optical thicknesses to 10%, except in cases of mistaken phase identification; most of the remaining bias is caused by differences between actual and assumed cloud particle sizes and the small effects of cloud variations at scales < 5 km. Global mean cloud properties averaged over the period July 1983–June 1994 are the following: cloud amount = 0.675 ± 0.012; cloud-top temperature = 261.5 ± 2.8 K; and cloud optical thickness = 3.7 ± 0.3, where the plus–minus values are the rms deviations of global monthly mean values from their long-term average. Long-term, seasonal, synoptic, and diurnal cloud variations are illustrated. The ISCCP dataset quantifies the variations of cloud properties at mesoscale resolution (3 h, 30 km) covering the whole globe for more than a decade, making it possible to study cloud system evolution over whole life cycles, watching interactions with the atmospheric general circulation. Plans for the next decade of the World Climate Research Programme require continuing global observations of clouds and the most practical way to fulfill this requirement is to continue ISCCP until it can be replaced by a more capable system with similar time resolutions and global coverage.

1. Introduction

The main impetus until now for the International Satellite Cloud Climatology Project (ISCCP) within the World Climate Research Programme (WCRP) has been to obtain more information about how clouds alter the radiation balance of Earth (Schiffer and Rossow 1983). To this end ISCCP[1] has been collect-

*NASA/Goddard Institute for Space Studies, New York, New York.
+NASA Headquarters, Washington, D.C.
Corresponding author address: Dr. William B. Rossow, NASA/GISS, 2880 Broadway, New York, NY 10025.
E-mail: wrossow@giss.nasa.gov
In final form 6 May 1999

[1]ISCCP Stage B3 data (reduced volume infrared and visible radiances) are produced from reduced resolution data supplied by the EUMETSAT for the Meteorological Satellite (METEOSAT); the Japanese Meteorological Agency (JMA) for the Geostationary Meteorological Satellite (GMS); the Atmospheric Environment Service of Canada for the Geostationary Operational Environmental Satellite-East (GOES-East); Colorado State University (CSU) for the GOES-West; and the National Oceanographic and Atmospheric Administration (NOAA) for the polar orbiters. The Centre de Meteorologie Spatiale at Lannion performs normalization of the geostationary satellite radiances to the afternoon polar orbiter and the National Aeronautics and Space Administration (NASA)/Goddard Institute for Space Studies produces the final data products. Additional ancillary data are supplied and all data products are archived by the NOAA National Environmental, Satellite and Data Information Service (NESDIS). The ISCCP data are also archived at NASA/Langley Research Center.

ing, since July 1983, the infrared and visible radiances obtained from imaging radiometers carried on the international constellation of weather satellites. After sampling the radiances to reduce data volume, they are calibrated, navigated, and placed in a common format. The first global radiance dataset was released in 1984 (Schiffer and Rossow 1985). These radiance data have been analyzed to characterize the main cloud radiative properties and their variations over the whole globe; the first cloud data products were released in 1988 (Rossow and Schiffer 1991). Specific accomplishments have been to extend the measured cloud properties beyond total areal cover and low-level cloud-base height, available from surface observations, to include cloud-top temperature and pressure (or height) and cloud optical thickness and to extend the range of observed cloud variations from diurnal and mesoscale to multiyear and global scales.

The ISCCP cloud datasets are now being used to determine cloud effects on Earth's radiation balance (see references in Zhang et al. 1995; Rossow and Zhang 1995); the outcome of these and other ongoing studies will allow an assessment of whether the main ISCCP objective has been (or will be) met. Clouds also play an equally important role in Earth's water cycle as the intermediate stage between the water vapor that evaporates from and cools the surface and the precipitation that heats the atmosphere and returns the water back to the surface. This water cycle is the other major energy exchange process in the climate besides radiation exchanges (Peixoto and Oort 1992). Variations in both the radiation and water cycles help drive the circulations of the atmosphere and oceans. Since it is the motions of the atmosphere that transport water vapor and form clouds and precipitation, understanding both the cloud radiation and the cloud water feedbacks on the climate also requires understanding how atmospheric motions determine cloud properties. These topics are now receiving more emphasis under the Global Energy and Water Experiment (GEWEX) component of the WCRP, particularly through its Cloud System Study (Browning 1993). Such considerations call for more information on how cloud systems form, evolve, and decay in different meteorological regimes, which requires extending the list of cloud properties that can be measured and organizing the observations in more meaningful terms of the evolution of the dynamics of whole systems, such as the midlatitude cyclones and tropical mesoscale convective complexes, which are readily recognized in Fig. 1. Research is under way to adapt or extend the ISCCP cloud datasets for this purpose (e.g., see Mapes 1993; Machado and Rossow 1993; Han et al. 1994; Lin and Rossow 1994; Lau and Crane 1995; Liu et al. 1995; Chen and Houze 1997; Sheu et al. 1997; Lin et al. 1998a,b; Machado et al. 1998; Han et al. 1999, manuscript submitted to *J. Atmos. Sci.*); Tselioudis et al. 1999).

Completion of the 8-yr cloud climatology (C-series datasets) in 1992 occasioned a review of ISCCP objectives and plans. Research had already provided estimates of the accuracy of the first cloud properties obtained by ISCCP and suggested that some improvements to the analysis method were possible. These improvements have now been implemented in the ISCCP analysis and are being used to produce a second version of the cloud products (D-series datasets). This paper is a progress report on ISCCP that describes the changes made to the cloud data products (section 2), examines the evidence that these changes are improvements (sections 3, 4, and 5), summarizes some results (section 6), and discusses plans for ISCCP through 2005 (section 7). Stage B3 data (reduced resolution, calibrated infrared and visible radiances) are currently available covering the period from July 1983 through December 1997 (Rossow et al. 1996a,b). The first cloud products (C series) are available for the period July 1983 through June 1991. The new version of the cloud products (D series) is being processed now and should be available for the period from July 1983 through December 1997 by late 1999 (Rossow et al. 1996c). A CD-ROM containing the monthly mean (D2) data for1989–1993 was released in December 1998; a CD-ROM containing data for 1983–88 will be released in summer 1999. Details of all the datasets, including browse images, calibration tables, complete documentation, up-to-date project status information, and information on how to obtain datasets (and CD-ROMs), can be found on the ISCCP Web site (http://isccp.giss.nasa.gov).

2. New datasets

The new ISCCP D-series cloud datasets differ from the previous C-series datasets because the analysis method has been changed in several ways and because more detailed results are reported (Rossow et al. 1996c). The main changes to the analysis method, which are discussed further in sections 3–5, are as follows.

1) Radiance calibrations have been revised slightly to remove spurious changes in the long-term

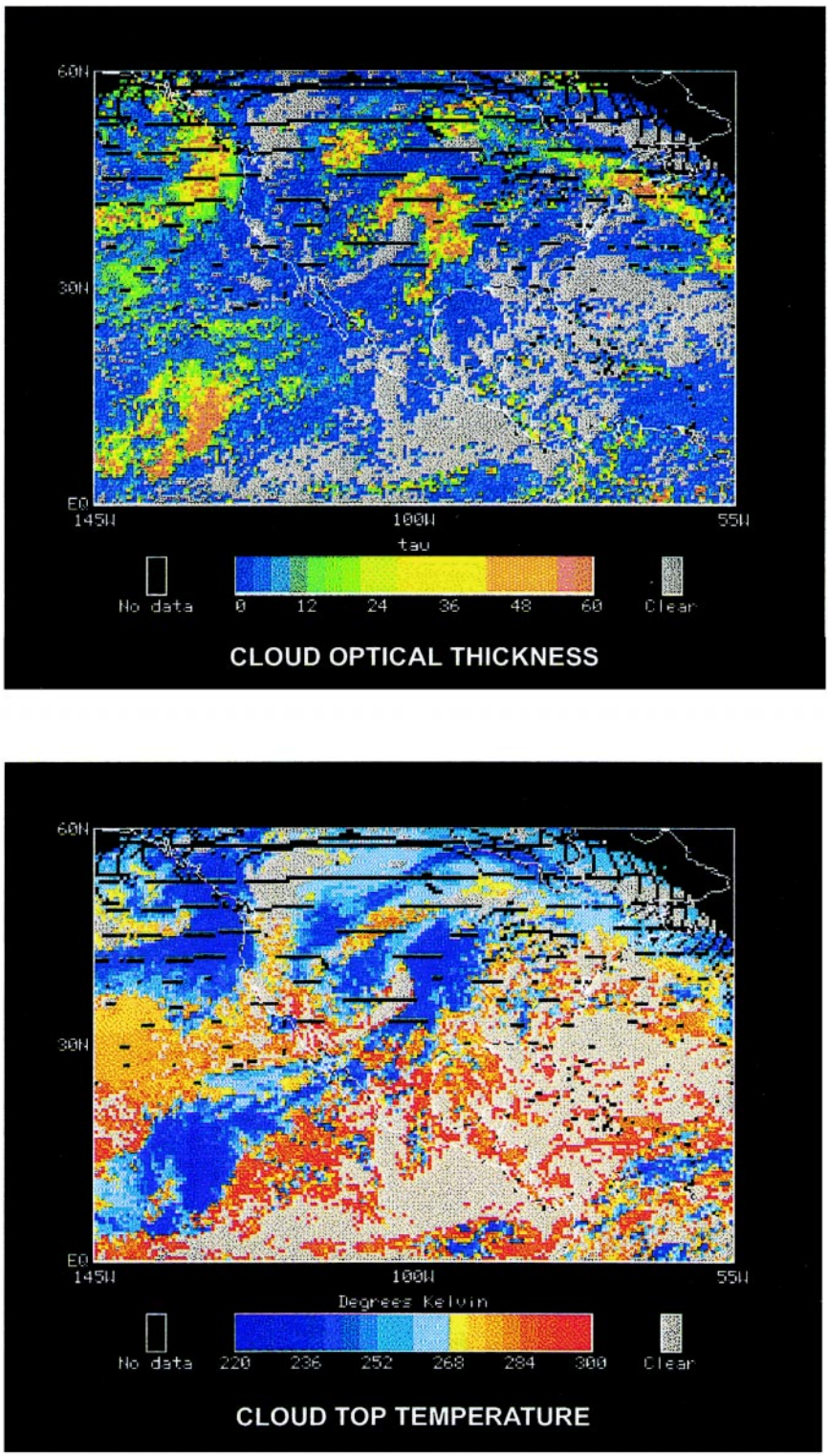

FIG. 1. ISCCP DX data from *GOES-7* for 13 March 1990 at 1800 UTC over North America showing the variation of cloud optical thickness (upper) and cloud-top temperature (lower) at about 30-km resolution associated with a midlatitude cyclone located over the central United States. The cold front and low pressure center are indicated by clouds with optical thickness > 30 and cloud-top temperatures < 240 K.

record and to reduce occasionally larger deviations for individual satellites.

2) Cirrus cloud detection sensitivity over land was increased by lowering the infrared (IR) radiance threshold from 6 to 4 K.
3) Low-level cloud detection sensitivity was increased at higher latitudes and near sunrise and sunset at all latitudes by changing the visible (VIS) radiance threshold test to a VIS reflectance threshold test.
4) Low-level cloud detection sensitivity over snow and ice in the polar regions was increased by lowering the visible (VIS) radiance threshold from 0.12 to 0.06, using a reflectance test instead of a radiance test, and by using a new threshold test on 3.7-μm radiances (near-IR radiances; NIR).
5) Biases in the cloud optical thickness (τ) and cloud-top pressures (P_c) of cold clouds (cloud-top temperature T_c < 260 K) were reduced by using an ice polycrystal microphysics model in place of a liquid droplet microphysics model.
6) Biases in cloud optical thicknesses over ice and snow surfaces were reduced by using an additional test on the 3.7-μm radiances.
7) Biases in cloud-top temperatures and pressures were reduced by including the effects of IR scattering.
8) Errors in surface and cloud-top temperatures were reduced by using a new treatment of the water vapor continuum absorption in the IR.

To provide more detailed information about the variations of cloud properties, the contents of the cloud products [Tables 1 and 2; cf. Tables 1 and 2 in Rossow and Schiffer (1991)] have been revised by adding a sixth τ category in the $P_c-\tau$ distribution reported in the 3-hourly D1 dataset (parallel to the C1 dataset), by adding a cloud water path (WP) parameter in the D1 dataset, by providing an alternative conversion of cloud-top pressure to height in meters above mean sea level, and by adding a cloud amount (CA) frequency distribution to the monthly mean D2 dataset (parallel to the C2 dataset).

The most notable change in content is to report the actual average physical properties (T_c, P_c, τ, WP) for 15 cloud types in the D1 dataset, in addition to their amounts, which also improves the accuracy of this information in the monthly mean D2 dataset. The cloud types are defined, as before, in terms of their cloud-top pressures and optical thicknesses (there are also three cloud types defined only by cloud-top pressure), but the $P_c-\tau$ categories have been changed slightly to make them simpler [Fig. 2; cf. Fig. 4 in Rossow and Schiffer (1991)]: there are now three optical thickness

TABLE 1. Contents of the ISCCP D1 dataset provided every 3 h for each 280-km grid cell over the globe. Some variables are defined only for local daytime and are undefined at night. Additional variables are calculated in the provided D1-READ program: cloud amounts, cloud-top height in m, total IR radiance, total VIS radiance, and layer midpoint pressures.

- Cloud amount and distribution information
  - Total number of pixels
  - Total number of cloudy pixels
  - Number of cloudy pixels and marginally cloudy pixels for various channel combinations
  - Number of cloudy pixels in seven PC categories (IR only)
  - Number of cloudy pixels in 42 PC/cloud optical thickness categories
  - Number of ice clouds in low- and middle-level categories
- Total cloud properties
  - Cloud-top pressure (PC) for various channel combinations
  - Cloud-top pressure for marginally cloudy pixels
  - Spatial standard deviation of PC
  - Cloud-top temperature (TC) for various channel combinations
  - Cloud-top temperature for marginally cloudy pixels
  - Spatial standard deviation of TC
  - Cloud optical thickness (TAU) for various channel combinations
  - Cloud optical thickness for marginally cloudy pixels
  - Spatial standard deviation of TAU
  - Cloud water path (WP) for various channel combinations
  - Cloud water path for marginally cloudy pixels
  - Spatial standard deviation of WP
- Cloud-type information
  - Average cloud-top temperatures for seven PC categories (IR only)
  - Average TC, TAU, and WP for cumulus, stratocumulus, and stratus clouds (liquid and ice)
  - Average, TC, TAU, and WP for altocumulus, altostratus, and nimbostratus clouds (liquid and ice)
  - Average TC, TAU, and WP for cirrus, cirrostratus, and deep convective clouds (ice)
- Surface properties
  - Surface pressure (PS) and skin temperature (TS)
  - Spatial standard deviation of TS
  - Surface visible reflectance (RS)
  - Spatial standard deviation of RS
  - Surface near-IR reflectance (RNIR)
  - Snow/sea ice cover fraction
  - Topography and land–water flag
- Radiances
  - Average IR radiance for cloudy pixels
  - Spatial standard deviation of cloudy IR radiances
  - Average IR radiance from clear-sky composite
  - Average IR radiance for clear pixels
  - Spatial standard deviation of clear IR radiances
  - Average VIS radiance for cloudy pixels
  - Spatial standard deviation of cloudy VIS radiances
  - Average VIS radiance from clear sky composite
  - Average VIS radiance for clear pixels
  - Spatial standard deviation of clear VIS radiances
  - Viewing geometry and day–night flag
  - Satellite identification
- Atmospheric properties
  - Near-surface air temperature (TSA)
  - Temperature for nine pressure levels
  - Tropopause temperature and pressure
  - Precipitable water amounts for five layers
  - Ozone column abundance
  - Source of atmospheric data

categories for both low-level and middle-level clouds, and the boundary between cirrus and cirrostratus has been made constant with pressure. In addition, separate results are reported for the liquid and ice forms of the low-level and middle-level clouds (all high clouds are assumed to be ice clouds).

Since even more detail is desired for regional studies of cloud behavior and cloud effects on other climate processes, the most detailed cloud product, DX data, which has a resolution of 30 km and 3 h, is now being archived at NASA/Langley (see ISCCP Web site for information). The DX dataset reports, for individual image pixels, the calibrated IR and VIS radiances (and radiances at any additional wavelengths), viewing/illumination geometry, the clear-sky radiances inferred by the analysis, the cloud-clear decision reached by the cloud detection algorithm, and the results of the radiative model analysis employing three different cloud models (Table 3). Figure 1 is based on a composite of DX data.

TABLE 2. Contents of the ISCCP D2 dataset provided every month for each 280-km grid cell over the globe; monthly average information is also provided at each of eight times of day. Cloud-top heights (in m) are calculated in the provided D2-READ program.

Cloud amount information
Total cloud amount (CA)
Marginal IR cloud amount
Frequency distribution of cloud amounts
Average total cloud properties
Cloud-top pressure (PC)
Time mean spatial standard deviation of PC
Temporal standard deviation of spatial mean of PC
Cloud-top temperature (TC)
Time mean spatial standard deviation of TC
Temporal standard deviation of spatial mean of TC
Cloud optical thickness (TAU)
Time mean spatial standard deviation of TAU
Temporal standard deviation of spatial mean of TAU
Cloud water path (WP)
Time mean spatial standard deviation of WP
Temporal standard deviation of spatial mean of WP
Average properties for cloud types (CA, PC, TC, TAU, WP)
Low, middle, and high clouds (CA, PC, and TC from IR only)
Cumulus, stratocumulus, and stratus clouds (liquid and ice)
Altocumulus, altostratus, and nimbostratus clouds (liquid and ice)
Cirrus, cirrostratus, and deep convective clouds (ice)
Average surface properties
Surface skin temperature (TS)
Standard deviation of TS
Surface visible reflectance (RS)
Snow/sea ice cover fraction
Average atmospheric properties
Surface pressure (PS)
Near-surface air temperature (TSA)
Temperature at 740 mb (T740), 500 mb (T500), and 375 mb (T375)
Tropopause pressure (PT) and temperature (TT)
Stratosphere temperature at 50 mb, ST50
Precipitable water for 1000–680 mb (PWL)
Precipitable water for 680–310 mb (PWU)
Ozone column abundance (O3)

3. Radiance calibration

The satellite imaging radiometers used by ISCCP are designed primarily to make pictures of changing cloud patterns associated with significant weather; consequently, accurate absolute calibrations were not emphasized. Moreover, although all the imagers have an infrared (IR wavelength $\approx$ 11 μm) and visible (VIS wavelength $\approx$ 0.6 μm) spectral channel in common, there are small differences in the actual wavelength responses (Rossow et al. 1996b). Therefore, ISCCP has had to conduct an extensive calibration effort to provide the absolute calibrations needed for retrieval of physical quantities from the measured radiances and to construct a uniform global dataset over a long time period by normalizing 25 (through 1998) different radiometers to the same calibration standard. The methods used and detailed results are reported in Rossow et al. (1987, 1992, 1996a), Brest and Rossow (1992), Desormeaux et al. (1993), and Brest et al. (1997), and can be found on the ISCCP Web site.

Post facto assessments of the C-series ISCCP cloud products showed some spurious changes in the retrieved cloud and surface properties that are caused by residual calibration problems. Systematic global changes occur suddenly when changing from one Advanced Very High Resolution Radiometer (AVHRR)

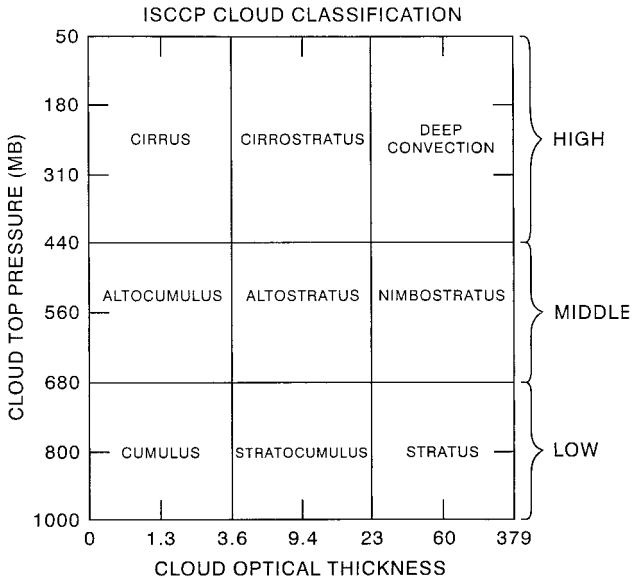

FIG. 2. New cloud-type definitions used in the ISCCP D-series datasets for daytime. All low and middle cloud types are separated into liquid and ice types; all high clouds are ice. Nighttime cloud types are low, middle, and high, as indicated on the right.

to the next (Klein and Hartmann 1993; Rossow and Cairns 1995; Brest et al. 1997; Bishop et al. 1997), causing apparent long-term trends in the cloud properties and the amounts of different cloud types. In addition, some occasional regional changes are apparent as discontinuities of retrieved quantities between adjacent areas observed by different geostationary satellites (Brest et al. 1997). The magnitude of these calibration artifacts is < 10%, which is the estimated uncertainty in the C-series calibrations; but one objective of reprocessing the ISCCP data is to reduce the magnitude of the systematic calibration artifacts by augmenting the normalization procedure (which is applied every month beginning in 1996) and reducing the global changes between different AVHRRs.

To normalize the calibrations of the series of AVHRRs on the NOAA polar orbiting weather satellites, the whole earth, excluding clouds, is assumed to represent a set of calibration targets that are more nearly constant in time as a statistical ensemble than any of the available radiometers or of any available calibrations of them. In other words, based on the post facto assessment, we conclude that the accuracy of independent calibrations attainable with today's satellite radiometers is less than that obtained by assuming that earth *as a whole except for clouds* does not change with time. This is a stricter assumption than made originally. Now, in effect, any real and systematic changes of the whole Earth become the (smaller) error. Even excluding the clouds in this procedure, these data cannot be used to monitor any *slow linear* trends of the global mean cloud properties retrieved from the radiances that might accompany a changing global climate (Rossow and Cairns 1995) because there is no independent confirmation of the long-term calibration. However, shorter-term (e.g., interannual or nonlinear decadal) and/or regional changes in clouds can now be reliably assessed with these data because we assume only that the whole earth is constant over the whole data record, which would remove only a linear trend in global mean quantities. After reprocessing, the remaining *systematic* errors in the relative calibrations at shorter timescales are reduced to < 3% for VIS and < 1% for IR (Brest et al. 1997). The ISCCP calibrations are now the most complete and self-consistent set of calibrations available for *all* of these radiometers: total *relative* uncertainties in the radiance calibrations are estimated to be 5% for visible and 2% for infrared; *absolute* uncertainties are < 10% and < 3%, respectively (Brest et al. 1997).

TABLE 3. Contents of the ISCCP DX dataset provided every 3 h at approximately 30-km intervals for individual satellites.

- Pixel identification information
  - Flags indicating day–night, land–water, near shore, high topography, snow/ice
  - Viewing geometry (satellite zenith, solar zenith, relative azimuth angles, sunglint flag)
- Original radiances (IR, VIS, NIR reflectivity, any others)
- Clear sky radiances (IR, VIS, NIR reflectivity)
- Cloud detection algorithm test results
  - Time and space tests
  - Clear sky composite tests
  - Radiance threshold results (IR, VIS, NIR)
- Radiative retrieval quality codes
- Surface temperature, pressure, and reflectance from clear sky composite radiances
- Surface temperature, pressure, and reflectance for clear pixels
- Blackbody cloud model results: top temperature and pressure
- Liquid cloud model results: top temperature, top pressure, and optical thickness
- Ice cloud model results: top temperature, top pressure, and optical thickness

4. Cloud detection and areal coverage

The ISCCP analysis begins by classifying each individual satellite field of view (pixel), about 4–7 km in size, as either cloudy or clear (Rossow and Garder 1993a). A pixel is called cloudy if the IR *or* VIS radiance differs from its corresponding clear-sky value (inferred from a statistical analysis of the radiance variations) by more than the detection threshold.[2] Clouds that produce radiance changes that are too small or of the wrong sign are not detected. Clouds are assumed to cover individual pixels completely, so fractional areal cloud cover (or CA, reported as values from 0 to 1) is determined only for larger areas (280 km across) in the ISCCP datasets by the fraction of all pixels in each area containing clouds. The precision of individual cloud cover values for these areas is determined by the total number of pixels collected; for the sampled ISCCP data at one time, this number ranges from 20 to 120, about 70 on average, giving a precision from 0.008 to 0.05, about 0.015 on average (cloud amounts are reported with precision of 0.005). The time-averaged cloud cover fraction for the 280-km regions can also be thought of as the product of the average instantaneous cloud cover fraction and the frequency of occurrence of clouds; but since the latter quantity is about 90% on average for this sized region, we refer to cloud "amount" throughout as equivalent to cloud cover fraction (see discussion in Rossow et al. 1993).

a. Assessment

The accuracy of the ISCCP cloud amounts depends on three factors: the validity of the cloud detection (whether a particular pixel actually contains cloud or not), the sensitivity of the cloud detection (how much cloud with what properties is detectable), and the accuracy of the areal cover fraction estimated by counting cloudy pixels with a finite resolution. The first two factors depend on the magnitude of the detection thresholds (cf. Rossow et al. 1985), which vary with scene type in the ISCCP analysis. Comparison with other measurements of the surface properties retrieved from the clear-sky radiances in the C-series results (Rossow and Garder 1993b) indicates that the VIS radiance thresholds used over oceans and land are about right, except at larger solar zenith angles where the constant-radiance threshold becomes equivalent to a much larger reflectance threshold, and that the IR radiance threshold used over ocean is about right but that it is too large over land. Over snow and sea ice, the VIS thresholds are too large. These results imply an underdetection of clouds in the C-series results by about 0.05–0.10 over land and by larger amounts in the polar regions, particularly during summertime when the predominant cloud type is very low level and optically thin.

Extensive comparisons of ISCCP cloud amounts have been made with three other cloud datasets that show that detection errors (first two factors: either spurious detections when no clouds are present or missed clouds) are the largest source of systematic error in the ISCCP results. Individual ISCCP observations matched with over 670 000 individual surface cloud observations, as well as comparisons with the surface-based cloud climatology (Warren et al. 1986, 1988), suggest that the ISCCP total cloud amounts are too low over land by about 0.10, somewhat less in summer and somewhat more in winter, and about right (maybe slightly low) over oceans (Rossow et al. 1993). Both surface observers (Hahn et al. 1995) and satellites miss some clouds at night, the latter because broken low-level clouds do not always exhibit enough contrast in IR to be detected (cf. Rossow et al. 1985); but this effect is reduced in the dataset by using the daytime difference between VIS/IR and IR results to estimate a correction (Rossow et al. 1993). Comparisons of ISCCP upper-level cloud amounts to those determined by the Stratospheric Aerosol and Gas Experiments (SAGE; Liao et al. 1995a) and by two different analyses of High-Resolution Infrared Sounder (HIRS) data (Jin et al. 1996; Stubenrauch et al. 1999a; see also Wylie and Wang 1997) suggest an underestimate of upper-level cloudiness by at least 0.05–0.10, most of which is caused by missed detections of very thin ($\tau \sim 0.1$ over ocean and ~ 0.3 over land) clouds (cf. Wielicki and Parker 1992).

Polar clouds present more extreme examples of all the detection problems: they form at low temperatures and low solar illuminations where satellite radiometer sensitivity is reduced; they may have the same temperature as the surface or higher temperatures in inversion situations (Key and Barry 1989; Yamanouchi and Kawaguchi 1992); and they may have similar or smaller reflectivities than the highly reflective ice/snow surfaces (Raschke et al. 1992). Consequently, cloud detection errors are expected to be larger in the polar regions (Rossow and Garder 1993a,b; see also

[2]The radiance threshold is sometimes defined as the radiance value that divides clear from cloudy pixels, but in our usage, the threshold is the *change* from the clear radiance required to detect a cloud.

Mokhov and Schlesinger 1993, 1994). Unfortunately, surface observations of polar clouds are also poor, partly because so few stations are located near the poles and partly because some conditions (particularly lack of illumination) create significant difficulties for surface observers, too (Hahn et al. 1995; Curry et al. 1996). Nevertheless, comparisons with surface observations in polar regions suggest that the ISCCP cloud amounts are probably too low by about 0.15–0.25 in summer (Schweiger and Key 1992; Rossow et al. 1993; see also Curry et al. 1996) and possibly too high by 0.05–0.10 in winter (Curry et al. 1996). Using only surface observations with sufficient sky illumination (Hahn et al. 1995) reduces the wintertime bias, however.

Although detection errors appear to be the largest source of bias in the ISCCP cloud amounts, the accuracy of individual determinations of cloud cover fraction depends on a complex interplay among the size distribution of cloud elements, the spatial resolution of the satellite sensor, the detection sensitivity of the analysis (dependent on cloud properties), the space–time sampling characteristics of the dataset, the size of the area (and the timescale) for which cloud property distributions remain roughly constant, and the size of the area in which cloud fraction is calculated. Di Girolamo and Davies (1997) have done the most rigorous study of the interaction of the first two aspects and Minnis (1989) examines the satellite-view-angle dependence that these two factors introduce: generally, cloud cover fraction is overestimated if the sensor resolution is larger than the most frequent cloud element size, an effect that grows worse for off-nadir views. Wielicki and Parker (1992) show that a finite detection threshold (third factor) offsets the overestimate produced by the first two factors because the occurrence of optically thin cloud elements is much more frequent for broken or scattered cloudiness (see also Chambers et al. 1997b). The precise balance between these offsetting effects depends on the size distribution and properties of the clouds (i.e., cloud type), but the results of Wielicki and Parker (1992) suggest that the overall bias of ISCCP low-level cloud cover fractions is < 0.1. All of these factors are combined when comparing the satellite cloud cover fraction, determined at a resolution of about 5 km for areas about 280 km across, with surface observations representing a resolution certainly better than 100 m covering an area about 30–50 km across. Such comparisons for scattered cloudiness show (ignoring false or missed detections) that, even though the sampling areas and resolutions differ by more than an order of magnitude, the satellite and surface-observed cloud cover fractions are about the same in the mean, but the rms differences in individual determinations of scattered cloudiness (i.e., fair weather cumulus) is about 0.25 (Rossow et al. 1993). Over all cloud types, the rms uncertainty in individual ISCCP cloud amounts appears to be about 0.15.

b. Changes

Changes have been made to the ISCCP cloud detection method (see section 2, Rossow et al. 1996c) to reduce some of the larger biases in total cloud amount discovered in the validation studies described above. The general low bias over land areas is reduced by decreasing the IR threshold from 6 to 4 K over land, which improves the detection of cirrus over land. The small low bias over high-latitude oceans is reduced by converting the VIS radiance threshold to a reflectance threshold, which is equivalent to a threshold decrease (this change also adds more clouds over high-latitude land areas). The general low bias over polar regions, particularly in summertime, is reduced by decreasing both the VIS and IR thresholds and adding an additional test on 3.7-μm wavelength radiances over ice/snow surfaces (cf. Yamanouchi and Kawaguchi 1992; Raschke et al. 1992). With the new thresholds, the detectable lower limits of cloud-top height (Z_c) and cloud optical thickness (τ) for complete cloud cover are approximately Z_c = 400 m (for $\tau \geq 3$) and τ = 0.15 over ocean, and Z_c = 600 m (for $\tau \geq 3$) and τ = 0.25 over land. For global mean cloud properties ($Z_c \approx 4300$ m and $\tau \approx 3.7$), the detectable limit of cloud cover fraction in individual pixels is about 0.1 over ocean and about 0.15 over land.

Individually matched C-series ISCCP and surface observations (predominately over land) show an asymmetric distribution of differences in total cloud amount because of the tendency for ISCCP to miss some clouds especially in winter [Figs. 1 and 5 in Rossow et al. (1993)]. The upper portion of Fig. 3 illustrates this result for January 1991: the differences between C1 and surface cloud amounts are most often nearly zero, but there are more negative than positive differences in all latitude zones, particularly at midlatitudes and even more so in the summer (south) polar region. The lower portion of Fig. 3 shows the same comparison using the new D1 data for the same month: the changes in detection threshold produce a difference distribution that is now more nearly symmetric about zero. Note that the total difference between the two datasets ("error") is not much reduced, but it is now almost entirely "random" (i.e., symmetrically distrib-

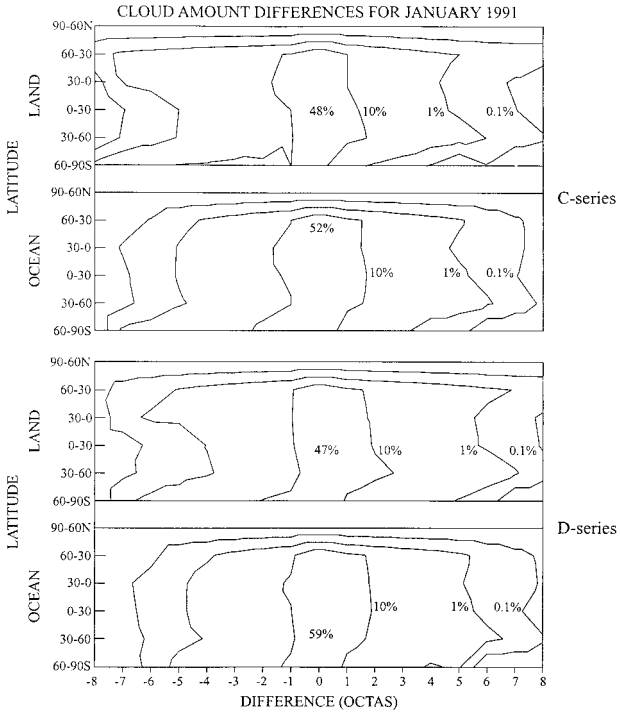

FIG. 3. Frequency contours of the distribution of differences (%) in instantaneous cloud cover fraction for 2.5° regions between the ISCCP C-series (upper two panels) and the D-series (lower two panels) and individually matched surface observations at all available weather stations over land and ocean for January 1991 in each latitude zone. Maximum values are indicated by numbers within the innermost contour. The comparison is restricted to sunlit areas, so there are no results north of 60°N.

uted about zero). The overall comparison of the C-series distribution of cloud cover fractions with those from (land) surface observers [Fig. 2 in Rossow et al. (1993)] also showed a tendency for the ISCCP results to overestimate cloud cover fractions that are < 0.5 and to underestimate cloud cover fractions that are > 0.5; but the new D-series cloud cover fraction distributions (not shown) exhibit no such discrepancy.

Figure 6 in Rossow et al. (1993) compares the zonal mean differences of total cloud amounts from ISCCP C2 and from the surface observations climatology. Comparing the ISCCP D2 data in the same way (not shown) shows that 1) the positive bias in ISCCP cloud amounts over oceans has increased very slightly; 2) the negative bias in ISCCP cloud amounts over land has changed to a positive bias that is about the same as over oceans; and 3) the negative bias in ISCCP cloud amounts in both polar regions is much reduced, especially when using only surface observations with sufficient night sky illumination, but the ISCCP values are still about 0.10 too low in summertime (see references in Curry et al. 1996). That the ISCCP cloud amounts are now consistently higher by about 0.05 than the surface observations over land and ocean for all seasons (except the summertime poles) is consistent with a slightly higher sensitivity of the satellite observations to the presence of optically thin cirrus, reinforced by a surface observer's tendency to underreport such clouds (Hahn et al. 1995), and with a tendency of the satellite to overestimate cloud amounts for low-level scattered cloudiness (cf. Wielicki and Parker 1992), offset by a surface observer's tendency to overreport such clouds (Hahn et al. 1995). Table 4 shows that most of the additional cloud over land appears as cirrus clouds, since they are detected only by the lower IR threshold (cf. Jin et al. 1996), whereas the additional cloud over oceans appears as low-level cloud, since they are detected only by the lower VIS threshold. Both of these changes are also shown specifically to improve the comparison of the ISCCP results with an analysis of HIRS observations (Stubenrauch et al. 1999a). In the polar regions, most of the additional cloud cover over snow and ice surfaces is low-level, optically thin cloud detected by threshold tests on the NIR radiances (cf. Raschke et al. 1992; Yamanouchi and Kawaguchi 1992), even though about half of these additional clouds were also detected by lowering both the VIS and IR thresholds in the original algorithm. Thus, the changes in detection thresholds for the D-series analysis have been successful in reducing the main biases of the C-series results found in validation studies.

5. Cloud physical properties

If an individual pixel is cloudy, then comparison of the observed radiances to those predicted by a radiative transfer model (Rossow and Schiffer 1991; Rossow et al. 1991) determines a cloud-top temperature (T_c) from the IR radiances (both day and night) and a visible optical thickness (τ) from the VIS radiance (daytime only, defined by cosine of the solar zenith angle, $\mu_0 \geq 0.2$). Atmospheric effects are accounted for and cloud-top pressure (P_c) is determined from T_c using an atmospheric temperature profile from the Television Infrared Observation Satellite (TIROS) Operational Vertical Sounder product produced by NOAA NESDIS. If the pixel is clear, then two surface properties are retrieved (Rossow and Garder 1993b): surface temperature (T_s) from the IR radiance, assuming an emissivity of unity, and surface visible reflec-

tance (R_s) from the VIS radiance during daytime, assuming that all surfaces are isotropic reflectors [however, an anisotropic reflection model is used for the retrieval of τ over oceans; Rossow et al. (1989)].[3]

In the radiative model, each pixel is assumed to be horizontally uniform and plane parallel. Atmospheric properties vary with height, but a cloud is assumed to be a single, vertically uniform or physically "thin" layer in the sense that there is no explicit dependence on layer vertical structure in the retrieval model. The radiation from each pixel is also assumed to be independent of its neighbors (no lateral exchange or transport of photons): this is the so-called independent pixel approximation, which has generally been used since the earliest satellite data analyses (see references in Rossow 1981; Rossow et al. 1985; Rossow et al. 1989). Thus, the retrieved cloud (and surface) properties are *radiatively weighted averages* over the small-scale ($\lesssim$ 5 km) variations present in each pixel (Rossow 1989).

In the C-series analysis model, all clouds are assumed to be composed of liquid water droplets (spheres) with a size distribution given by the gamma function defined by an effective (mean) radius, r_e = 10 μm, and an effective variance of 0.15 (Hansen and Travis 1974). Cloud water path in grams per meter squared is given by WP = $(0.692\tau)r_e = 6.292\tau$. Mie scattering at VIS wavelengths ($\approx$ 0.6 μm) is treated as conservative; weak scattering at IR wavelengths ($\approx$ 11 μm) is neglected. The cloud optical thickness at IR wavelengths, τ_{ir}, is related to the optical thickness at VIS wavelengths by an empirical formula: $\tau_{ir} = \tau/2.0$ (see references in Rossow et al. 1989; Minnis et al. 1993b).

TABLE 4. Comparison of global, annual mean quantities from the ISCCP D2 and C2 datasets for 1986.

Statistic	C2 value	D2 value	Change
Total cloud amount (%)	63.4	68.6	+5.2
Average over ocean	71.2	73.0	+1.8
Day–night difference	–2.3	–2.1	+0.2
Average over land	46.1	58.9	+12.8
Day–night difference	+6.3	+5.4	–0.9
Average over North Pole	52.0	68.3	+16.3
Average over South Pole	52.6	68.6	+16.0
Average over north midlatitudes	64.8	71.9	+7.1
Average over south midlatitudes	81.0	82.5	+1.5
Average over Tropics	59.4	62.4	+3.0
Cloud-top temperature (K)	262.8	261.5	–1.3
Average over ocean	266.6	264.7	–1.9
Day–night difference	+1.2	+1.9	+0.7
Average over land	254.6	253.9	–0.7
Day–night difference	+12.0	+12.2	+0.2
Cloud-top pressure (mb)	600	580	–20
Average over ocean	642	619	–23
Day–night difference	+3	+4	+1
Average over land	507	496	–11
Day–night difference	+97	+86	–11
Cloud optical thickness	5.7	3.8	–1.9
Average over ocean	5.3	3.8	–1.5
Average over land	6.9	3.8	–3.1
Cloud water path (g m^{-2})	–	65	–
Average over ocean	–	61	–
Average over land	–	74	–
Surface temperature (K)	289.3	289.3	0.0
Average over ocean	290.7	291.2	+0.5
Day–night difference	+2.0	+1.5	–0.5
Average over land	285.2	285.8	+0.6
Day–night difference	+15.0	+15.0	0.0

a. Assessment

Three situations bracket the range of uncertainties in retrieved values of T_c: low-level clouds with distinct tops and moderate-to-large optical thicknesses; high-level, diffuse-topped clouds with moderate-to-large optical thicknesses; and high-level, optically thin clouds. In the first two cases if $\tau \gtrsim 5$, the observed IR radiance is emitted solely from the upper portion of

[3]Since clear radiances are inferred for every pixel, these surface properties are retrieved from the clear-sky radiances for every pixel, whether it is clear or not.

TABLE 4. *Continued.*

Surface reflectance	0.16	0.17	+0.01
Average over ocean	0.12	0.12	0.0
Average over land	0.27	0.28	+0.01
Cirrus and cirrostratus properties			
Amount (%)	14.2	19.6	+5.4
Top temperature (K)	233.8	227.5	–6.3
Top pressure (mb)	295	267	–28
Optical thickness	3.3	2.2	–1.1
Water path (g m^{-2})	–	23	–
Deep convective properties			
Amount (%)	5.2	2.6	–2.6
Top temperature (K)	235.7	234.8	–0.9
Top pressure (mb)	318	326	+8
Optical thickness	30.3	35.6	+5.3
Water path (g m^{-2})	–	261	–
Middle-level cloud properties			
Amount (%)	18.1	19.0	+0.9
Top temperature (K)	264.7	262.8	–1.9
Top pressure (mb)	565	557	–8
Optical thickness	6.7	4.8	–1.9
Water path (g m^{-2})	–	60	–
Low-level cloud properties			
Amount (%)	26.4	27.5	+1.1
Top temperature (K)	280.5	281.1	+0.6
Top pressure (mb)	814	826	+12
Optical thickness	5.3	4.7	–0.6
Water path (g m^{-2})	–	51	–

the cloud with no significant contribution (< 10% for $\tau = 5$) of radiation transmitted from below the cloud; hence, the retrieval of T_c does not depend on the cloud optical thickness. We defer discussion of the third case, where the retrieval does depend on optical thickness, until after discussion of errors in the optical thickness values.

In the first case, the cloud top is distinct in that optical thickness increases from zero to a moderately large value over a very small vertical extent [say < 30–100 m; see Minnis et al. (1992)]. In this case, the ISCCP determination of T_c from the observed IR emission should be most accurate (representing an average of small-scale variations in the location of cloud top). The main sources of error in T_c are from radiometer calibration (< 1.5 K; Brest et al. 1997), the radiative transfer model treatment of cloud emission and scattering, the treatment of water vapor absorption/emission above the cloud, and errors in the atmospheric temperature–humidity profiles. The latter two error sources are important only for low-level clouds at lower latitudes; but since the atmospheric corrections (difference between T_c and the IR brightness temperature) are typically only a few kelvins, the latter two errors are only 1.5 K. Neglect of IR scattering causes an overestimate of T_c that is only about 0.5–1.0 K for low-level clouds, but can be a few degrees for higher-level clouds. Careful comparison of marine stratus cloud tops determined in the new ISCCP dataset with collocated measurements made during the First ISCCP Regional Experiment in 1987 (FIRE 87; Randall et al. 1996) and the Atlantic Stratocumulus Transition Experiment (Wang et al. 1999) shows agreement of T_c values to within 1.0–1.5 K, similar to results obtained by Minnis et al. (1992). However, the ISCCP values of P_c for persistent marine stratus clouds are too low by 50–80 mb (Wang et al. 1999) because of systematic errors in the TIROS Operational Vertical Sounder atmospheric temperature profiles (Stubenrauch et al. 1999a). Comparison of the geographic distributions of monthly mean cloud-top pressures for all low- and middle-level clouds from ISCCP with those inferred from rawinsonde humidity profiles shows agreement to within about 25–50 mb (Wang and Rossow 1995; Wang 1997).

In the second case, the cloud top is "diffuse" in that the cloud optical thickness increases slowly from the top downward over a considerable vertical extent. In this case, the emission arises from within the cloud at a larger temperature than the temperature at the precise physical top defined by the limit of the cloud mass. Although the ISCCP value of T_c will represent the observed emission, this "radiative" cloud-top height will be biased low. Using the limb-viewing observations by SAGE, Liao et al. (1995b) determined that this type of cloud top is encountered above the 440-mb level almost 70% of the time in the Tropics with an average P_c discrepancy of about 150 mb, but only about 30%–40% of the time at higher latitudes

with an average P_c discrepancy of about 50 mb. In this case, the ISCCP "cloud top" has to be interpreted as the location where "significant" cloud mass is first encountered when moving downward through the atmosphere.

The main source of bias in the retrieved optical thicknesses comes from differences between the actual and model-specified cloud microphysical properties (we discuss the effects of subpixel-scale inhomogeneity below). In the C-series products, all clouds are assumed to be composed of 10-μm liquid water spheres. For liquid water clouds that are actually composed of spherical droplets (those with $T_c \geq 273$ K at least), the main error comes from differences between the actual and model-specified effective droplet radii, r_e: retrieved optical thicknesses increase (decrease) by about 15% for a factor of 2 decrease (increase) of r_e (Rossow et al. 1989; Nakajima and King 1990). If droplet size varies vertically within the cloud, the error is still given approximately by the average of the errors in each sublayer (cf. Sun and Shine 1995). Direct retrievals of cloud-top droplet sizes in liquid water clouds by Han et al. (1994, 1995) show that the actual global monthly mean value of $r_e \approx 11$ μm, about 12.5 μm over oceans and about 8.5 μm over land, implying biases of the ISCCP optical thicknesses of −4% over ocean and +2% over land (Han et al. 1994). Variability among individual clouds implies rms uncertainties of τ of about ±12% (Han et al. 1994). Descloitres et al. (1998) directly test the scattering phase function used in the ISCCP analysis by comparison with multi-view-angle measurements from an aircraft-borne Polarized and Directionality of the Earth's Reflectance (POLDER) instrument (similar results have been obtained from the space-borne instrument as well; F. Parol 1998, personal communication): the average angle dependence of visible radiances reflected from liquid water clouds predicted by the ISCCP model matches the observations to within a few percent.

Scattering from spherical liquid water particles was not expected to represent the scattering by ice clouds very accurately, but in 1982 little was known about the general particle size and shape distributions in such clouds or how to treat their scattering more accurately. Minnis et al. (1993b) and Descloitres et al. (1998), for example, show that the liquid water droplet model disagrees with observations of visible radiances reflected from cirrus clouds by 10%–20% or more. Hence, major field experiments were undertaken to improve knowledge of cirrus cloud properties, sponsored by the United States (FIRE; Randall et al. 1996), by several European countries (International Cirrus Experiment and European Clouds Radiation Experiment; Raschke et al. 1990, 1998), and by Japan (Japanese Cloud-Climate Study). These experiments led to development of several theoretical scattering phase functions for different ice particle shapes (Takano and Liou 1989; Muinonen et al. 1989; Macke 1993; Iaquinta et al. 1995; Macke et al. 1996) that compare more favorably with the observations (Foot 1988; Francis 1995; Spinhirne et al. 1996; Descloitres et al. 1998). Minnis et al. (1993a,b) demonstrated the significant improvement in the retrieved values of τ and T_c for optically thin cirrus when the scattering phase functions of hexagonal crystals (Takano and Liou 1989) are used instead of the function for spherical droplets. Mishchenko et al. (1996) shows that, although differing in detail, the scattering phase functions of hexagonal crystals and the fractal crystal shape proposed by Macke (1993) produce similar results when averaged over the globe and time. Based on the study by Minnis et al. (1993a), the ISCCP C-series values of cirrus cloud τ are biased high by 30%–40% and the cloud-top heights are biased low by about 1 km (or T_c is biased high by about 7–10 K). The latter estimate is consistent with that obtained from a comparison of ISCCP high-level cloud tops and those measured by SAGE (Liao et al. 1995b).

At night, only IR radiance measurements are available to ISCCP, so that cloud-top location can only be estimated from the IR radiance assuming that the cloud is opaque. During daytime, when VIS radiance can be used to determine τ, the value of T_c is corrected for transmitted radiance assuming no other cloud layer is present below (Rossow et al. 1989; Rossow et al. 1991). Comparison of daytime C-series results obtained with and without the use of VIS data suggests an overall bias of nighttime cloud-top pressures of about +50 mb. This is an underestimate of the effect because of the incorrect microphysics assumed for ice clouds and because the ISCCP correction procedure underestimates the correction when another cloud is present below an optically thin, upper-level cloud, which occurs about 25% of the time (Jin and Rossow 1997). Analysis of infrared sounder data, which is much less sensitive to cloud microphysics and underlying clouds, indicates a bias of the C-series ISCCP cloud-top pressures at night of +75 mb on average (Stubenrauch et al. 1999a).

At the beginning of ISCCP in 1982, another source of uncertainty in the retrieved cloud properties came from a lack of understanding of the nature and magnitude of the effects of "small-scale" spatial variabil-

ity on radiative transfer through clouds. Most recent studies have focused on the effects at solar wavelengths where they are expected to be largest (Cahalan et al. 1994a; Kobayashi 1993; Marshak et al. 1995; Barker 1996; Davis et al. 1997; Loeb and Coakley 1998; Marshak et al. 1998; Cairns et al. 1999), but Barker and Wielicki (1997) and Stubenrauch et al. (1999b) consider the effects of vertical and horizontal variability at 100-km scale on infrared radiation. Monte Carlo calculations for marine boundary layer clouds suggest that there could be angle-dependent errors up to 10%–30% in optical thickness values retrieved from area-averaged visible reflectances when the *pixel-to-pixel* cloud variations in marine boundary layer clouds are not properly accounted for in the area-averaged radiation (Kobayashi 1993; Loeb and Coakley 1998); however, the larger estimates in this range are obtained when *subpixel* radiance variations are attributed solely to cloud cover variations (cf. Coakley and Bretherton 1982), rather than to optical thickness variations as ISCCP does (Loeb and Coakley 1998). This result might be explained by the results from studies using 30-m resolution Landsat data that show that the subpixel (i.e., scales 5 km) radiance variations cannot be attributed completely to cloud cover variations (Wielicki and Parker 1992; Chambers et al. 1997b). In any case, and regardless of which of these two interpretations is more accurate, the higher-resolution studies also show very clearly that the magnitude of the cloud variations at scales smaller than about 5 km contributes little to the total cloud variability (Chambers et al. 1997b; Barker 1996). In other words, the radiative effects of cloud variations at scales smaller than a typical satellite pixel are smaller than the available estimates because the cloud variability *within* pixels is smaller in magnitude than the variability *between* pixels. Cahalan et al. (1994) and Chambers et al. (1997a) also show that the independent pixel approach accounts for the cloud variations over larger scales (50–100 km) with good accuracy, but that the area-averaged radiation is more accurately determined from the logarithmic average optical thickness rather than the linear average. Thus, the cloud optical thicknesses obtained by ISCCP, while still uncertain for individual pixels because of small-scale effects including partial cloud cover, provide an accurate representation of area-averaged cloud radiative effects that accounts for most of the small-scale cloud variability by a radiatively weighted (essentially logarithmic) average of individual pixel values.

b. Changes

The major change made in the D-series analysis is to use a separate ice cloud microphysics model for retrieval of optical thicknesses and top temperatures for colder clouds. Ice clouds are identified as having $T_c < 260$ K and are assumed to be composed of fractal polycrystals (Macke et al. 1996) with a –2 power-law size distribution between 20 and 50 μm, giving an effective radius $r_e = 30$ μm, and an effective variance of 0.1 (see Mishchenko et al. 1996). The choice of this mean value of r_e is based on early results from a near-global survey of ice cloud particle sizes (Han 1999, personal communication); however, the resulting scattering phase function for visible radiation is not very sensitive to the particle size distribution, except in the forward scattering direction, which is not encountered in satellite data (Mishchenko et al. 1996). The value of τ_{ir} is obtained from calculations by Minnis et al. (1993a) of infrared absorption and scattering by ice spheres, since particle shape effects are weak at wavelengths ≈ 11 μm: $\tau_{ir} = \tau/2.13$. The empirical factor relating τ and τ_{ir}, used for all clouds in the C series, is replaced by a more accurate value for liquid water clouds (based on Mie scattering calculations): $\tau_{ir} = \tau/2.56$. Ice water path (IWP) for the fractal shape depends on the product of the ratio of the ice particle's volume to cross section (0.615 times that for a sphere; A. Macke 1994, personal communication) and its bulk mass density [0.85 g cm^{-3}, in the middle of observed values (Hobbs 1974)]: the product is an "effective" density, taken to be 0.523 g cm^{-3}, within the range given by Heymsfield (1972). Thus, IWP = $(0.350\tau)r_e$, which becomes IWP = 10.5τ for 30-μm particles.

The choice of a value of $T_c = 260$ K to separate ice and liquid water clouds is based on the analysis of ISCCP and microwave water paths by Lin and Rossow (1996) that shows that the ratio of liquid water path (from microwave) to the total cloud water path (from visible reflectances) falls below 50% at about this temperature on average. This result is also consistent with collections of in situ detections of liquid water droplets in clouds over a wide range of temperatures from at least 227 to 273 K (Feigelson 1984).

Descloitres et al. (1998) show that the new ice scattering phase function used by ISCCP represents the average angle dependence of visible radiances reflected from cirrus clouds to within a few percent (roughly similar results have been obtained with the spaceborne POLDER instrument; F. Parol 1998, personal communication). Table 4 shows the changes in average high-level cloud properties between the

C-series and D-series results. Globally, cirrus and cirrostratus (see Fig. 2) optical thicknesses have been reduced by about 30% and their top temperatures lowered by about 6 K (cloud-top pressures reduced by about 30 mb), consistent with the bias estimates of Minnis et al. (1993a). These changes also improve the agreement between the ISCCP D-series data and a matched analysis of the HIRS data by the 3I method, both in terms of the amount of transparent clouds and their average emissivities (Stubenrauch et al. 1999a,b).

Because clouds reflect sunlight with a different angular distribution than snow and ice surfaces, some clouds appear darker than the background at some scattering geometries as directly observed (Raschke et al. 1992). In such cases there can be two values of the cloud optical thickness that are consistent with the observed reflectance. In the C-series analysis, polar clouds are assumed to be composed of liquid water droplets and the snow and ice surfaces are assumed to be Lambertian, both of which exaggerate the difference in reflectivities. Moreover, the larger possible value is always selected. Both of these factors contribute to a significant overestimate of polar cloud optical thicknesses in the C-series results (Curry et al. 1996). In the new D-series analysis, this bias over snow and ice surfaces is reduced by using the more accurate ice crystal scattering phase function and using reflected sunlight measured at 3.7-μm wavelength to select one of the two possible optical thickness values consistent with the visible reflectance (Rossow et al. 1996c). A further reduction might be obtained using a more realistic reflectance function for the surface. The improvement is shown by two characteristics of the new results. First, the distribution of cloud optical thicknesses obtained at viewing geometries where two values are possible now better resembles the distribution obtained at geometries where only one value is possible. Second, as Fig. 4 shows, the D-series results greatly reduce a large "diurnal" variation of cloud optical thicknesses at higher latitudes in the C-series results, which is likely spurious in winter but partly real in summer. Overall, the average optical thicknesses of polar clouds in the D-series results (Fig. 5c) are in better qualitative agreement with other available estimates (cf. Curry et al. 1996).

Another (small) change in the D-series analysis is to include the effects of infrared scattering by clouds. Since the scattering operates more on the transmitted radiation, the effect is larger when the contrast between the cloud emission temperature and the temperature

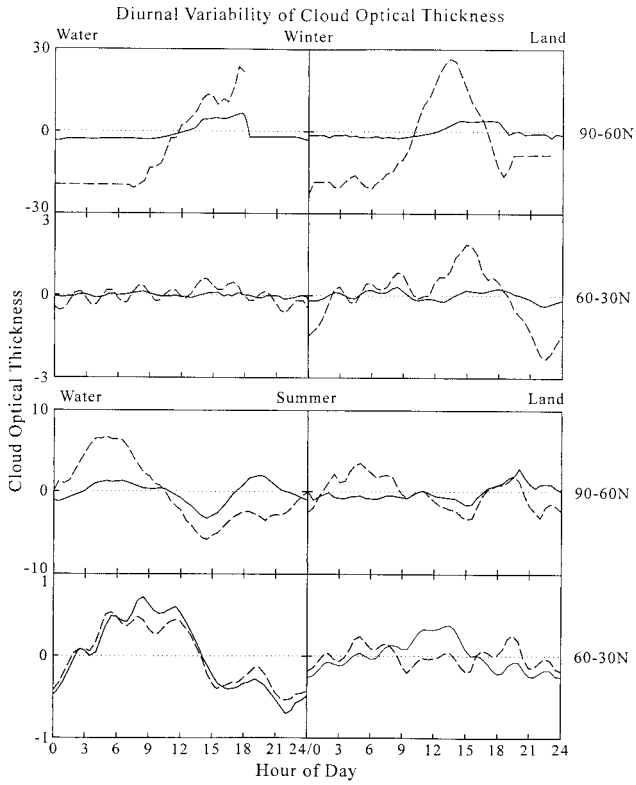

FIG. 4. Seasonal mean diurnal cycle of cloud optical thicknesses in two latitude bands in the Northern Hemisphere for winter (upper two panels) and summer (lower two panels) over ocean and land from the ISCCP C2 (dashed line) and D2 (solid line) datasets, expressed as difference from the average over the whole day. Note changes of vertical scale with latitude and season.

of the infrared radiation coming from below the cloud is larger and decreases with increasing cloud optical thickness. Note that this effect is usually neglected in satellite cloud retrievals, so that, even for marine stratus clouds (the best case), the effect can represent a negative bias of cloud-top heights of as much as 50–100 m (Wang et al. 1999). In general, this correction decreases cloud-top temperatures by only 1–2 K for high-level clouds with $\tau \gtrsim 6$.

6. New results

a. Average cloud properties

Table 4 compares global, annual mean results from the new ISCCP D-series with the previous C-series results (cf. Rossow and Schiffer 1991) for the common year 1986, which had no change in radiance calibration. The global annual mean cloud amount is about 0.69, 0.05 larger than before because of an increase of cloud amount over land by 0.13 and over the polar

regions by 0.16. The global land–ocean contrast in cloud amount has been reduced from 0.25 to about 0.14, in better agreement with surface observations (Warren et al. 1986, 1988) and analyses of HIRS data (Wylie et al. 1994; Stubenrauch et al. 1999a). The mean difference between daytime cloud amount and nighttime cloud amount (corrected using the daytime difference between VIS/IR and IR cloud amounts) is about the same as before and in good agreement with the revised surface observations (Hahn et al. 1995): over land, daytime cloud amount exceeds nighttime by about 0.05 and over ocean nighttime cloud amount exceeds daytime by about 0.02. These opposite variations cancel in the global mean. Midlatitude cloud amount exceeds that in the Tropics and polar regions, but the latitudinal contrasts have generally been reduced, except between northern midlatitudes and the Tropics. Polar cloud amounts are now slightly larger than the tropical cloud amount. Overall, Southern Hemisphere cloud amount still exceeds the Northern Hemisphere value, but the difference has been reduced to 0.04 from 0.06.

The global annual mean cloud-top pressure P_c is 580 mb, 20 mb lower than before because the higher-level clouds, now treated with a more realistic ice microphysics model, have somewhat higher tops (Table 4). This change is also reflected in the global mean cloud optical thickness, $\tau = 3.8$, which is about 67% of its previous value (Table 4). The global land–ocean contrast of cloud-top pressures is about the same as before with average values over land being 123 mb lower than over ocean. Most of this difference occurs because the topographic height of the land precludes cloud-top pressures > 900 mb in many places, but it is reinforced by a tendency for proportionately less lower-level and more high-level cloudiness over land than ocean in general, and for low-level clouds over land to extend to larger heights than low-level clouds over oceans (cf. Warren et al. 1986, 1988). On the other hand, the land–ocean contrast in cloud optical thicknesses has been eliminated in the new results. This change is caused primarily by the significant increase in the amount of thin cirrus cloud detected over land with the lower IR threshold, but there is also propor-

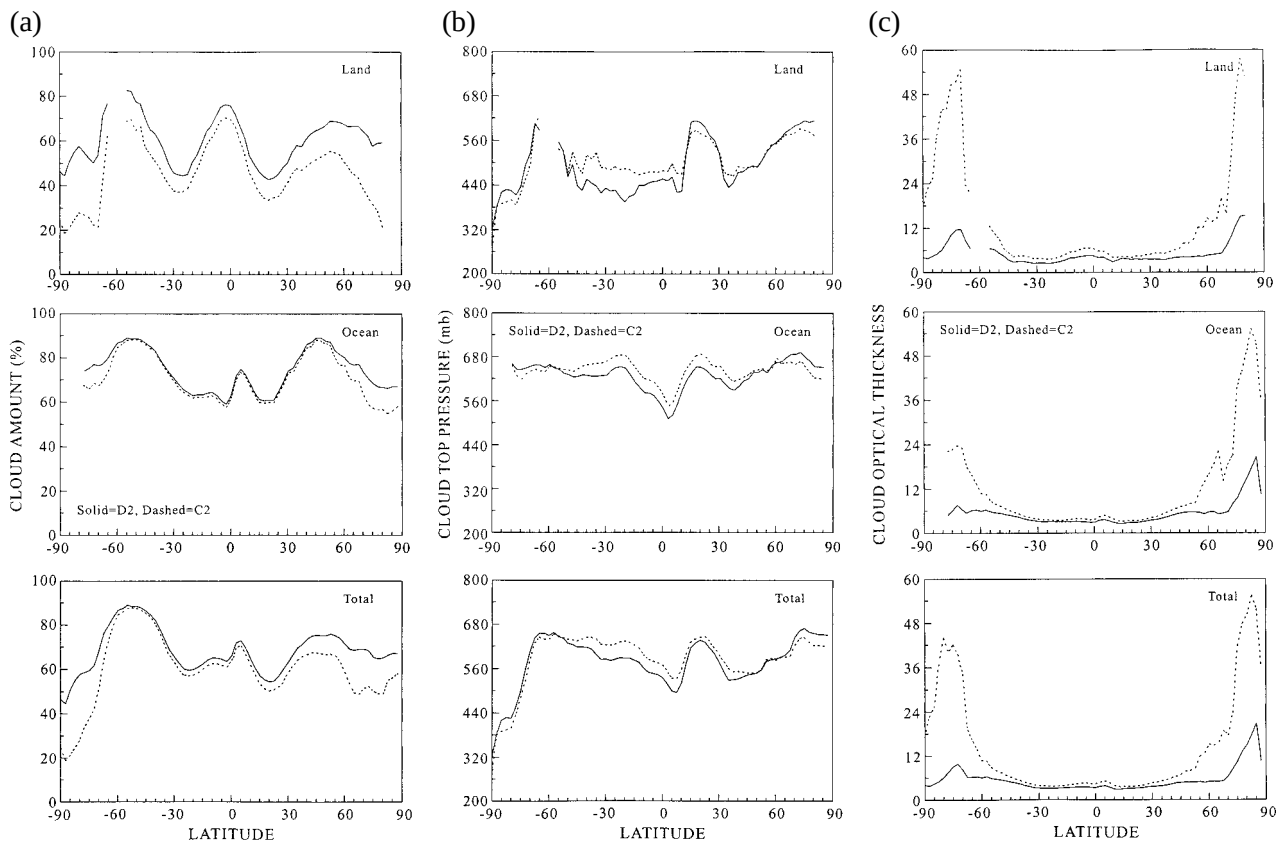

FIG. 5. Annual, zonal mean cloud properties over land and ocean and at all longitudes (total) from the ISCCP C2 (dashed line) and D2 (solid line) datasets for July 1990 through June 1991: (a) cloud amount (%), (b) cloud-top pressure in mb, and (c) cloud optical thickness.

tionately more ice cloud than liquid cloud over land than over ocean.

Figure 5 compares the zonal annual mean cloud amount, top pressure, and optical thickness from the D-series and C-series results based on a common period from July 1990–June 1991 (see also Doutriaux-Boucher and Seze 1998). The largest changes in cloud amount, as discussed in the previous section, appear in the polar regions and over land areas. At low and middle latitudes, the new cloud-top pressures are lower by 20–40 mb; but they are higher by 10–30 mb in the polar regions. A general decrease of P_c is caused by the new ice microphysics treatment, but this effect is reduced slightly over oceans by a small change in the atmospheric temperature profile and the detection of slightly more low-level cloudiness by the visible reflectance threshold test. Over land, the change in P_c is reinforced at lower latitudes by the increased detection of thin cirrus clouds; but over the Sahara (latitude 20°–30°N), some of the extra clouds are low-level cloud that may be mistaken identifications of dust storms (cf. Stubenrauch et al. 1999a). At lower latitudes, the new optical thicknesses are reduced from about 6 to about 4; the change over land is enhanced by detection of more cirrus. Note that the latitudes where the ITCZ occurs are clearly marked by a mini-

TABLE 5. Summary of new cloud climatology for 1986–93 in terms of annual means. Total cloud amounts are based on daytime and nighttime results, whereas cloud-type amounts are daytime only. Cloud-type amounts are for ice clouds; amounts in parentheses are for liquid clouds. Geographic regions are defined by the following latitude bands: tropical = ±30°, midlatitudes = 30°–60°, and polar = 60°–90°.

Quantity	Land	Ocean	Total
Global cloud and surface properties			
Cloud amount (%)	58.4	71.7	67.6
Cloud-top temperature (K)	253.1	266.0	262.1
Cloud-top pressure (mb)	490	625	583
Cloud optical thickness	3.8	3.9	3.9
Cloud water path (g m^{-2})	75.5	61.4	65.8
Surface temperature (K)	284.7	290.2	288.8
Surface reflectance	0.28	0.13	0.17
Global cloud-type amounts (%)			
Cumulus	1.2 (6.8)	1.3 (13.2)	1.2 (11.3)
Stratocumulus	0.9 (6.7)	0.9 (13.2)	0.9 (11.2)
Stratus	0.3 (1.5)	0.2 (1.8)	0.2 (1.7)
Altocumulus	5.5 (2.9)	5.0 (4.8)	5.1 (4.2)
Altostratus	4.0 (4.0)	3.8 (3.9)	3.8 (4.0)
Nimbostratus	1.3 (1.5)	0.9 (0.9)	1.0 (1.1)
Cirrus	15.8	12.0	13.2
Cirrostratus	5.3	6.0	5.8
Deep convection	2.5	2.7	2.6

Cloud type amounts (%)	Tropical	Northern midlatitudes	Southern midlatitudes	North polar	South polar
Cumulus	0.0 (12.3)	1.6 (10.7)	1.4 (15.1)	4.2 (3.6)	6.2 (2.2)
Stratocumulus	0.0 (10.7)	0.8 (10.9)	0.9 (16.8)	3.8 (7.7)	5.2 (4.0)
Stratus	0.0 (0.8)	0.2 (2.2)	0.2 (2.1)	1.3 (5.2)	1.1 (2.5)
Altocumulus	0.9 (6.1)	7.6 (3.2)	8.3 (2.8)	12.1 (0.6)	14.4 (0.1)
Altostratus	0.1 (4.7)	5.0 (4.2)	7.1 (4.2)	10.6 (1.4)	12.5 (0.3)
Nimbostratus	0.0 (1.0)	1.6 (1.7)	1.6 (1.2)	3.3 (1.5)	2.9 (0.2)
Cirrus	15.6	13.8	9.2	8.7	8.7
Cirrostratus	5.5	6.9	7.6	2.4	3.4
Deep convective	2.7	3.3	3.0	0.9	0.8

mum in the zonal annual mean distribution of cloud-top pressures, but there is only a very small maximum of the zonal annual average optical thicknesses in this zone. The optical thickness maximum is more pronounced in a zonal monthly mean. The midlatitude storm tracks do not produce very distinctive cloud property extremes in the annual mean. Table 5 summarizes the D-series global annual mean values for the period 1986–93.

In the polar regions the effect of the ice microphysical model on cloud-top pressure is overwhelmed by the detection of more clouds, which are necessarily low level because they were not detected in the IR. The most dramatic changes in cloud optical thicknesses occur in the polar regions, where mean values are now ≈ 4–20 instead of 20–55, because of the ice microphysics model and the procedure using the 3.7-μm radiances to resolve ambiguous cases. The latter effect seems more important. The new results are much closer than the previous results to the few other determinations of cloud optical thicknesses available for high-latitude areas. Analysis of radiometersonde data for eight overcast cases in austral winter over the South Pole in the early 1960s gave average cloud visible optical thicknesses of about 2 (roughly estimated from a broadband longwave emissivity of about 0.6) and cloud-top temperatures of ≈ 220 K (Stone 1993). In contrast, Lubin and Harper (1996) analyze one year (1992) of AVHRR images at the South Pole, reporting much lower average cloud-top temperatures in wintertime (≈ 180–200 K) and a mean visible optical thickness of about 1 (based on a narrow band infrared emissivity of ≈ 0.4). The difference in date may be significant if polar stratospheric clouds in association with the ozone hole are a relatively recent phenomenon. Ricchiazzi et al. (1995) report that clouds near the Antarctic coast in spring have much larger visible cloud optical thicknesses, ≈ 25. Annual average ISCCP results show a general decrease of cloud optical thickness from about 8–12 near the Antarctic coast to about 4–6 at the South Pole, with wintertime average cloud-top temperatures at the South Pole of 229 K; however, the wintertime ISCCP results are obtained only from the sunlight periods at the beginning and end of the winter. The apparent overestimate of optical thicknesses by ISCCP in the interior may be related to a systematic underdetection of thinner clouds there.

Leontyeva and Stamnes (1994) at Barrow, Alaska, and Barker et al. (1998) at 21 Canadian stations both infer summertime cloud optical thicknesses using surface total flux radiometers for selected *overcast* cases, finding *linearly* averaged visible optical thicknesses of 10–35. The average ISCCP results for collocated sites and the same time periods give average visible optical thicknesses of 7–16; however, when only total overcast cases are selected (about 25%–65% of the time period), the average optical thickness is 10–23, indicating a strong dependence on sampling that has not been entirely removed from this comparison. The D-series results agree somewhat better with those of Barker et al. (1998), even though values were reduced by the microphysics model, because the visible radiance calibration for this time period was changed so as to increase optical thicknesses. Nevertheless, there is a rough factor of 2 difference between the ISCCP results, based on measured *visible reflectances,* and the surface-based results, based on *diffuse broadband transmission.* Since the latter quantity is very sensitive to the assumed single scatter albedo of the cloud particles and other sources of absorption in the cloud outside the visible wavelength range (such as water vapor, which is represented in the surface analysis only by a climatology), the difference may be accounted for, in part, by errors in absorption and, in part, by the effects of cloud variations over spatial scales of 100–300 km. Although these very limited comparisons cannot confirm the accuracy very well, the ISCCP cloud optical thicknesses are now at least roughly similar in magnitude (within a factor of 2) in the polar regions, instead of being very much larger as they were in the C-series results.

b. Long-term variations

Figure 6 shows the long-term changes in global monthly mean cloud amount, top temperature, and optical thickness from both versions of the ISCCP analysis. Small differences (0.01–0.02) are caused by the changed detection sensitivity for the D series, which does not produce geographically uniform changes. Both versions show a notable slow change of global mean cloud amount occurring during the eight years, July 1983–June 1991. One interpretation of the cause of this variation is that it is related to the El Niño events in 1982–83, 1986–87, and 1991–92 (Rossow and Cairns 1995); however, a simple version of this explanation would predict an increase of global cloud cover in 1992–93 that does not appear. Note however, that El Niño variations of upper-tropospheric water vapor abundances exhibit different patterns for the past few events (Bates et al. 1996); thus, the failure of the simple expectation does not preclude an

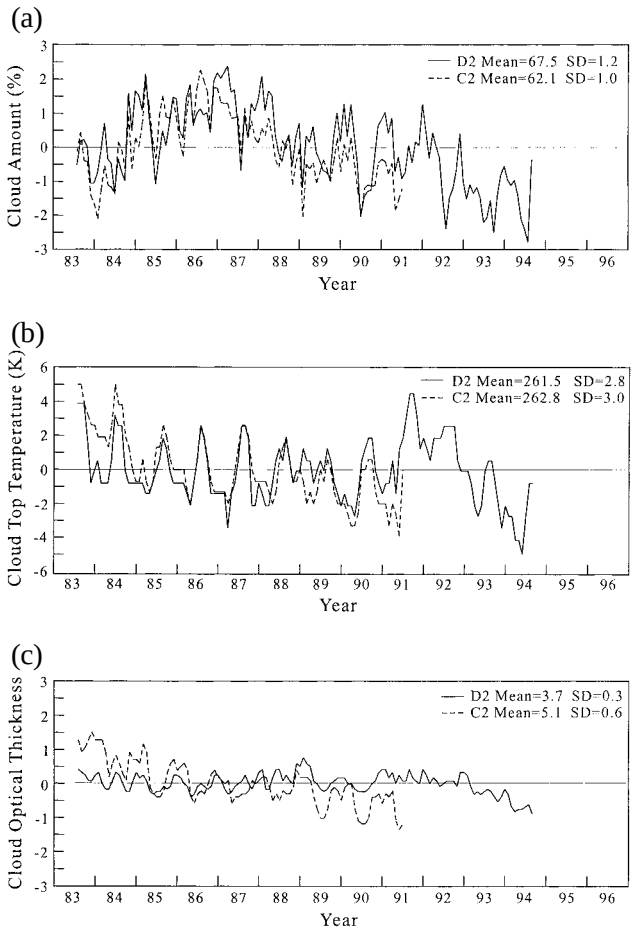

FIG. 6. Deviations of global monthly mean cloud properties from their long-term averages [indicated by means with standard deviations (SD)] for the ISCCP D2 (solid line) and C2 (dashed line) datasets: (a) cloud amount (%), (b) cloud-top temperature (K), and (c) cloud optical thickness.

El Niño explanation. Moreover, events in 1991–93 are complicated by the stratospheric cloud produced by the eruption of the Mount Pinatubo volcano, as we discuss below (just as the El Chichón eruption may confuse the interpretation of the 1982–83 El Niño). The data record is still too short to be sure of any interpretation. Another notable change in the results is the elimination of trends in cloud-top temperature and optical thickness that were caused by spurious changes of the radiance calibrations in the first results.

Figure 7 suggests that the production of large amounts of stratospheric aerosol by the Mount Pinatubo volcano in late 1991 may be associated with a decrease in cirrus cloud amounts by 0.02–0.04 [and an increase in their average optical thickness, first pointed out by B. Soden (1998, personal communication)], a possible example of an "indirect" aerosol effect on climate. However, the corresponding and opposite change of cumulus cloud amounts, together with the fact that both changes occur preferentially over oceans, argues that these changes may be caused directly by detection of the aerosol in the satellite visible radiances without any actual change of the clouds. In the ISCCP analysis over ocean, the clear-sky VIS reflectance is constrained by a model of ocean surface reflectance, so that some of the additional VIS reflectance caused by the aerosol could be detected as cloud by the VIS channel but not the IR channel; hence these "clouds" would be identified as low-level, optically thin clouds (which we call cumulus). The optical thickness of all other, already detected clouds would also be increased by the extra aerosol scattering, decreasing the amount of cirrus by shifting them to thicker and lower cloud-type categories. Over land, where the clear-sky VIS reflectance is determined from the data for each month, the main effect of the aerosol increase is to increase the land surface visible reflectances by about 0.02 in 1992; however, there is still a small increase of cirrus optical thicknesses that may be consistent with some observations during the FIRE Cirrus II experiment (Sassen and Cho 1992). An analysis of HIRS data suggests an increase of cirrus cloud amount(Wylie et al. 1994), consistent with an analysis of a high cloud index based on outgoing longwave radiation (Song et al. 1996). Both of these results probably include clouds that are too thin for ISCCP to detect, but whether they are clouds or aerosols is ambiguous. Further studies combining all available satellite observations are required to determine what actually happened.

c. Seasonal variations

Figure 6 also shows changes in the annual cycle of global mean cloud properties between the C-series

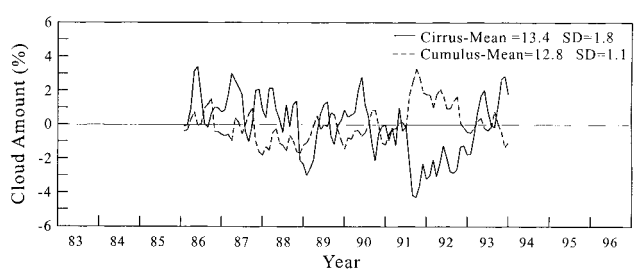

FIG. 7. Deviations of global monthly mean cirrus (solid line) and cumulus (dashed line) cloud amounts (%) from their long-term averages (shown as means with standard deviations) from the ISCCP D2 dataset (see Fig. 2 for definitions). Mount Pinatubo erupted in June 1991.

and D-series results: the annual cycle of global mean cloud amount is somewhat more regular, that of cloud-top temperature is a little less regular, and that of cloud optical thickness has been nearly eliminated in the new results. The first and second changes are associated with the enhanced detection of clouds over land, which increases the contribution of the land annual cycle (mostly Northern Hemisphere) to the global mean annual cycle of cloud amount but compensates for the effect of ocean–land contrast for cloud-top temperature. The third change is associated with the large reduction of the mean optical thicknesses of polar clouds, which reduces their contribution to the annual cycle (since there is no sunlight in wintertime, no values are obtained in that season), and with the increased detection of cirrus over land.

The mean annual cycle of zonal mean cloud amount in the D-series data is qualitatively the same as in the C-series data. The most prominent variations (±0.07) still occur over land in the Tropics (±15° latitude) and subtropics (±15°–30° latitude), caused by the hemispheric switching of the ITCZ and monsoons (Rossow et al. 1993). The annual variations of cloud amount over the ocean are only ±0.02. These low-latitude variations nearly cancel in the global mean. Midlatitudes exhibit a slightly smaller seasonal variation (±0.04 over ocean and land) with peak values occurring in (local) spring. The polar regions show a much smaller seasonal variation (±0.04) than before, in better agreement with surface observations (Curry et al. 1996), except the winter–summer contrast is still opposite in sign to that determined from surface observations due to an underestimate of summertime cloud amounts. The seasonal amplitude of total cloud amount decreases with latitude, whereas that for surface temperatures increases with latitude, more so in the land-dominated Northern Hemisphere than in the Southern Hemisphere.

The annual cycle of zonal mean cloud-top temperatures resembles that of zonal mean surface temperature, increasing amplitude with latitude. There is still a noticeable variation of cloud-top temperatures in the Tropics (±5 K over land but only ±2.5 K over oceans) despite the almost complete lack of an annual variation of surface (and atmospheric) temperature there (in fact there is a semiannual variation of ±1 K in surface temperature). Figure 8 shows the mean annual cycle of cloud-top temperature and pressure in the Tropics and midlatitudes. The cloud-top temperature variations at lower latitudes are caused almost solely by changes in cloud-top pressure associated with the shifting locations of the ITCZ. At higher latitudes, the annual

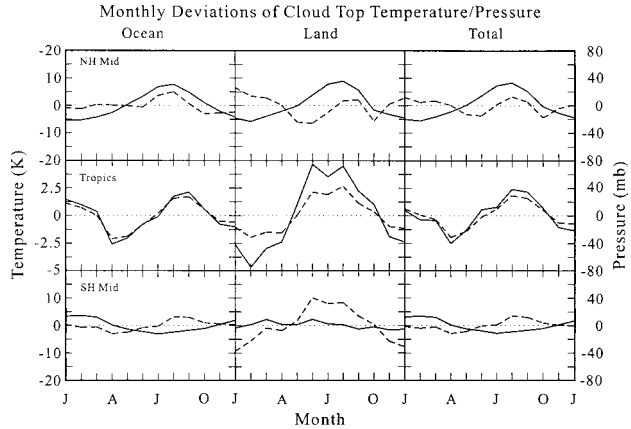

FIG. 8. Mean annual cycles of cloud-top temperature (K) (solid lines, left scale) and cloud-top pressure (mb) (dashed lines, right scale) over ocean, land, and all locations (total) as deviations from the annual averages for the period 1989–93 from the ISCCP D2 dataset. The three rows of panels show results for the northern midlatitudes (30°–60°N), Tropics (15°N–15°S), and southern midlatitudes (30°–60°S), top to bottom, respectively. Note changes of temperature scale at different latitudes.

variations of cloud-top temperature are caused in part by seasonal changes of air temperature at constant pressure, offset by seasonal variations of cloud-top pressure. In northern midlatitudes, the annual cycle of cloud-top pressure is shifted in phase from that of the atmospheric temperature so that the cloud-top temperature lags that of the surface and atmosphere. In southern midlatitudes, cloud-top pressure variations almost completely eliminate the annual variations of cloud-top temperature. A notable feature is that the annual variations of cloud-top pressures over land and ocean have opposite phases in the subtropics (Fig. 9). The largest annual variations of cloud-top pressure occur over Antarctica (±130 mb) associated with the seasonal appearance of polar stratospheric clouds, which may be only partly captured in the ISCCP dataset (cf. Lubin and Harper 1996).

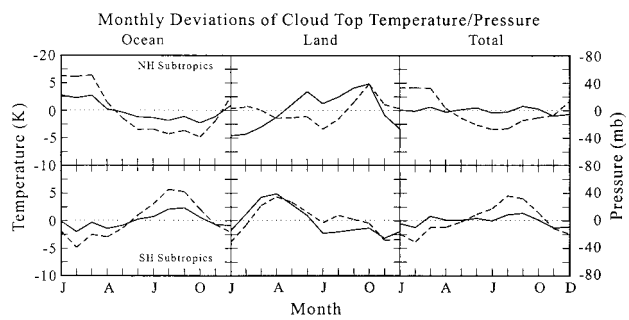

FIG. 9. Same as Fig. 8 but for the northern subtropics (15°–30°N; top row) and southern subtropics (15°–30°S; bottom row).

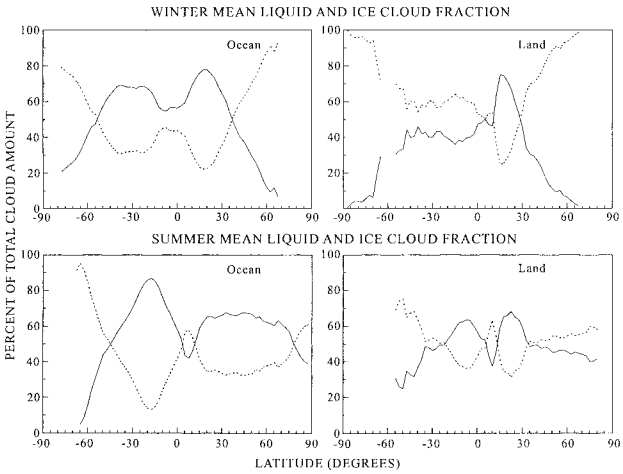

FIG. 10. Zonal mean fraction (%) of all clouds that are liquid (solid line) or ice (dotted line) for boreal winter and boreal summer seasons over ocean and land from the ISCCP D2 dataset for the period 1989–93.

Cloud optical thickness exhibits little (±0.5–2.0) seasonal variability except in the polar regions. These small variations at lower latitudes generally exhibit summer–autumn minima and winter–spring maxima, consistent with the results of Tselioudis et al. (1992). Since the polar averages are restricted to the sunlit areas, the winter values are estimated by interpolation, giving a maximum cloud optical thickness in Arctic springtime of about 24 and a minimum wintertime value of about 12, more than twice the estimates by Curry and Ebert (1992). Antarctic values range from a summertime maximum of about 12 to a wintertime minimum of about 4.

Figure 10 shows the seasonal variation with latitude of the relative amounts of ice and liquid water clouds that are obtained with the simple cloud-top temperature threshold used in the D-series analysis. At latitudes equatorward of about 35°, the majority of clouds are liquid water over oceans but ice over land, essentially in proportion to the relative amounts of low-level and higher-level clouds. Given the underestimate of low-level cloud amounts obtained from the "top-down" satellite view, this result suggests that liquid water cloud amounts are generally larger than ice cloud amounts. Lin and Rossow (1996) estimate the total ice cloud water path to be about 0.7 of the total liquid cloud water path in nonprecipitating clouds. In the Northern Hemisphere (mostly land), ice clouds predominate over liquid clouds poleward of about 35°N in wintertime (boreal seasons in the figure), whereas in the Southern Hemisphere (mostly ocean), ice clouds predominate over liquid clouds at all latitudes in local wintertime, consistent with generally higher cloud tops in this season. While these results are plausible, they need to be verified by direct determinations of cloud phase, preferably together with vertical profiles of cloud water amount throughout the depth of the atmosphere.

d. Diurnal variations

The diurnal variations of total cloudiness in the D-series results are quantitatively similar to the C-series results (Rossow et al. 1993; Kondragunta and

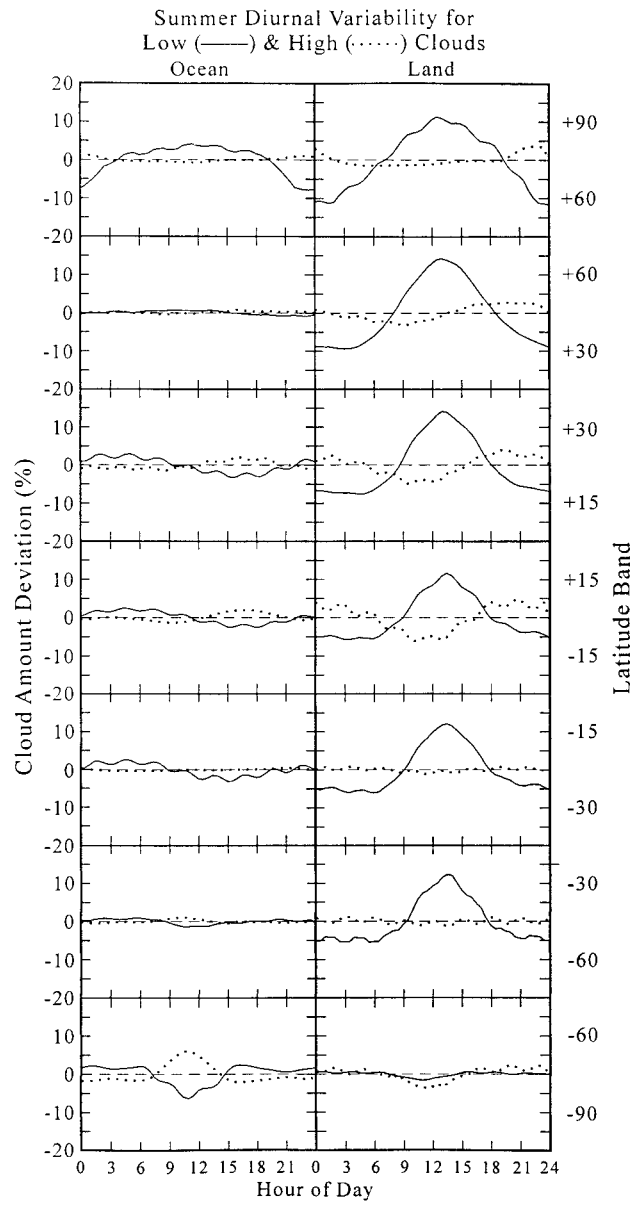

FIG. 11. Seasonal mean diurnal variations of low-level (solid line) and high-level (dotted line) cloud amounts (%) for various zonal bands over ocean and land for boreal summer from the ISCCP D2 dataset for the period 1989–93.

Gruber 1994; Cairns 1995), except for some changes caused by added cirrus clouds over land areas. The most notable features of diurnal cloud variations are the significant differences between the diurnal phases of low-level and upper-level clouds and between low-level clouds over ocean and over land (Cairns 1995). Such changes in the relative amounts of the different cloud types imply complex feedbacks on the radiation budget (cf. Chen et al. 1999). Figure 11 illustrates the shifting relative amounts of high- and low-level clouds over the diurnal cycle for boreal summertime (the average low-level cloud amount is about 30% larger than the average high-level cloud amount; see Table 5). Since the average amount and diurnal amplitude of high-level cloudiness are ≈ 0.2 and ≈ 0.1, respectively, the diurnal variations in low-level cloudiness do not appear to be caused simply by changing high-level obscuration and are in good agreement with surface observations (cf. Hahn et al. 1995; Rozendaal et al. 1995). The diurnal variations of low-level clouds are largest at low latitudes, although a similar variation occurs over midlatitude land, especially in local summertime; but the diurnal phase over the ocean is opposite to that over land: low-level cloud amounts peak near dawn over ocean but in late afternoon over land. High-level clouds generally have a smaller diurnal variation amplitude and significantly different phases than the low-level cloud variations: high-level clouds peak in early evening over both land and ocean. The variations in the polar region, shown in Fig. 11, occur in part because the geographic coverage provided by sun-synchronous polar orbiting satellites in the polar regions is not complete at each time of day, so that the portion of the area observed varies with time of day.

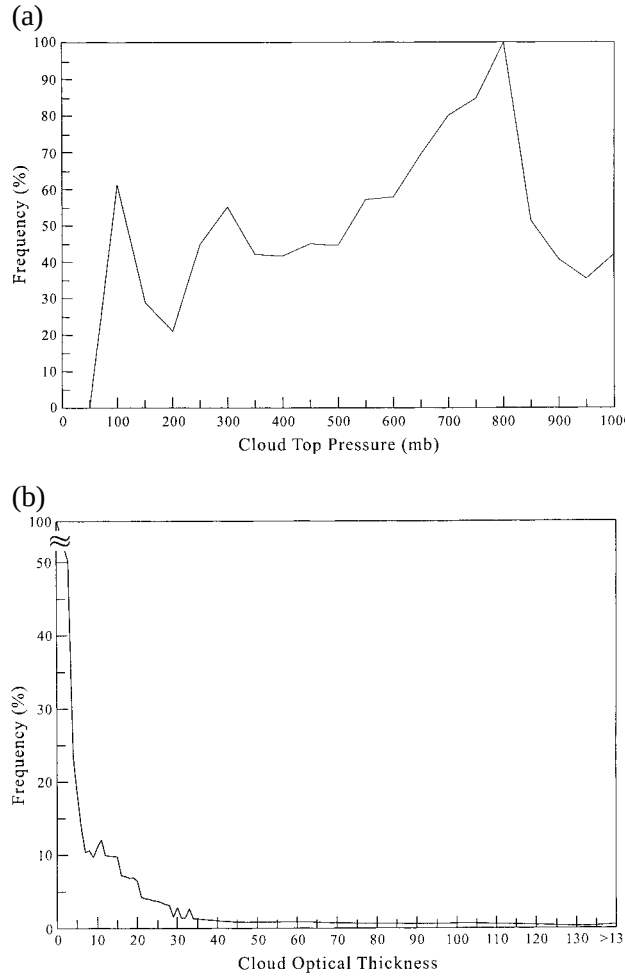

FIG. 12. Global frequency distributions, normalized to 100, of (a) cloud-top pressures (mb) and (b) cloud optical thicknesses from January and July 1994 as a representative example.

e. Cloud dynamics

The most difficult part of the cloud–climate feedback problem is to understand how atmospheric motions produce clouds and precipitation, especially since cloud systems exhibit characteristic structures and evolution on scales ranging from that of individual buoyant parcels (~ 500 m and ~ 10 min) to that of midlatitude baroclinic waves (~ 5000 km and ~ 5 days). The study of "cloud dynamics" has been conducted for decades using surface (mostly land based) and aircraft measurement campaigns, but observing the complete structure and following the whole evolution of the larger cloud systems has not been possible. The advent of global satellite observations with the requisite detail now makes it possible to observe the whole structure of both small and large cloud systems, to follow their whole life cycle, and to watch their interactions with each other and the atmospheric general circulation. Moreover, systematic satellite observations can be used to generalize the previous results with a much larger, statistically significant, number of cases covering all climate regimes. Some good examples of such uses of satellite data are 1) the studies of tropical convection by Mapes (1993), Laing and Fritsch (1993a,b), Chen et al. (1996), Chen and Houze (1997), and Machado et al. (1998); 2) studies of marine boundary layer clouds by Rozendaal et al. (1995), Minnis et al. (1992), and Wang et al. (1999); 3) studies of cirrus clouds by Wylie et al. (1994) and Jin et al. (1996); and 4) studies of midlatitude cloud systems by Lau and Crane (1995), Klein and Jacob (1999), and Tselioudis et al. (1999).

These detailed studies of the dynamics of specific types of cloud systems must ultimately explain why

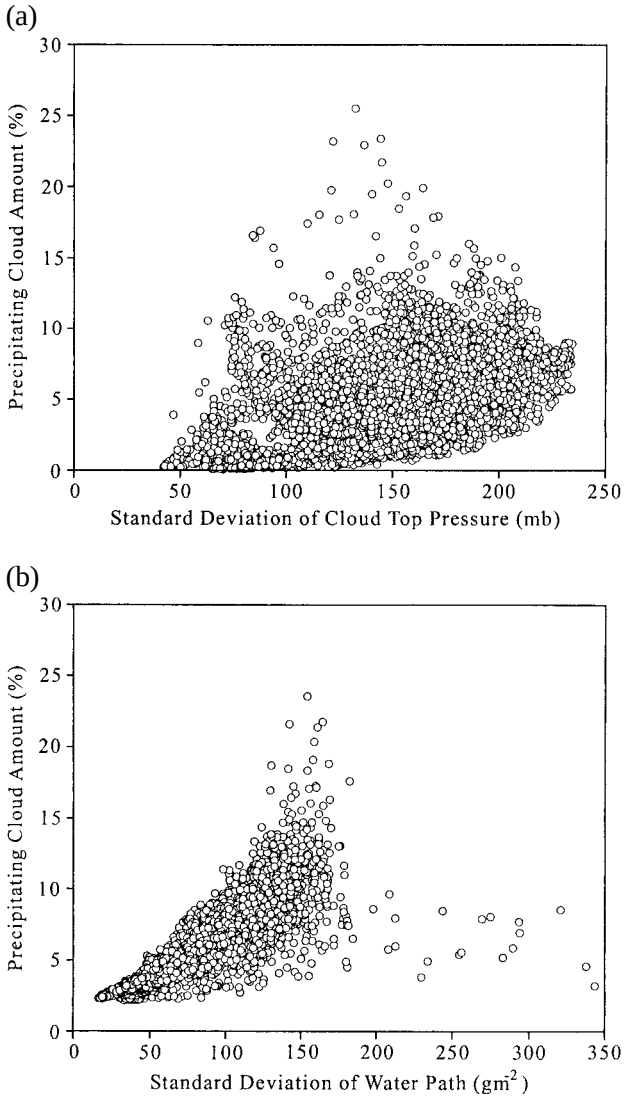

FIG. 13. Average monthly mean amount of "precipitating" clouds (deep convective and nimbostratus) compared with monthly total standard deviations of (a) cloud-top pressure (mb) and (b) cloud water path (g m^{-2}) based on data from 1986 to 1993. The standard deviations are caused predominantly by time variations at spatial scales $\geq$ 280 km. The linear correlation is (a) 0.40 and (b) 0.83.

the atmospheric general circulation produces the particular global distribution of cloud properties now defined by the cloud climatologies from satellite (ISCCP) and surface observations (Warren et al. 1986, 1988), in combination with information derived from rawinsonde humidity profiles (Wang et al. 1999, manuscript submitted to *J. Climate*). Together, these climatologies indicate that the most common clouds are low-level, liquid clouds (Fig. 12a): low-level cloud amounts are about 40% larger than high-level cloud amounts. Figure 12b, showing the global distribution of cloud optical thicknesses, indicates that the most common cloud is also optically thin: about 85% of all clouds have water paths $\leq$ 150 g m^{-2}, whereas less than 10% of clouds have water paths large enough to produce precipitation, $\geq$ 250 g m^{-2} (cf. Tian and Curry 1989; Lin and Rossow 1994, 1997). Thus, cloudiness on earth can be described as a persistent (frequency of occurrence is about 90% at 280-km resolution) and extensive (mean fractional cover is > 0.5 at 280-km resolution) background of optically thin clouds that determine the radiation balance of earth, together with a rare, highly variable component of precipitating clouds that are very sparse and intermittent in occurrence (total amount < 0.1). The skewed distributions of cloud-top pressure and optical thickness also mean that the variability of these parameters about their mean values is governed by variations of the amount of high-topped, optically thick clouds out of proportion to their relative amounts. Figure 13 shows that the standard deviations of cloud-top pressure and water path (dominated by time variations rather than spatial variations at scales < 280 km) are correlated with the amount of deep convective and nimbostratus (i.e., precipitating) clouds present. (Some of the cases with precipitating cloud amount > 0.15 are located over high mountains and may not represent actual precipitation. The few values of the standard deviation of water path > 200 g m^{-2} are located over Antarctica and may indicate a small number of erroneous retrievals.) Because there is a large amount of optically thin clouds, the linear correlation of cloud-top pressure is much weaker (r = 0.40) than for water path (r = 0.83). A complete understanding of cloud dynamics will explain why clouds are generally optically thin and why precipitating clouds are so rare. The nature of the linkage between cloud radiative and cloud-precipitation feedbacks is also determined by the answer to these questions.

7. Project plans

Under current plans, ISCCP will continue through 2005, but a discussion of the reasons for continuing or stopping a data analysis project can be instructive. The most obvious programmatic reason for continuing ISCCP is to provide cloud datasets for the ongoing WCRPs, now organized under GEWEX and the Climate Variability program (CLIVAR). Within the overall strategy of WCRP, GEWEX (initiated in 1988) coordinates studies of the "fast" climate feedback pro-

cesses involving radiation, clouds and rain, evaporation, and freshwater storage, with a special focus on land–atmosphere interactions. Studies of thermodynamics of the atmosphere and interactions with the earth's surface include problems ranging from the global radiation balance to cloud system dynamics. Significant progress has been made on the problem of clouds and radiation, but much more work remains and is only just beginning on understanding the role of clouds in the global hydrological cycle. The main effort of GEWEX toward this goal during the period from 1995 through 2005 will include at least five, possibly six, major regional hydrological experiments that will integrate surface and atmospheric observations from extensive sets of surface-based sensors and a whole new set of satellite sensors now being launched. CLIVAR (initiated in 1996) organizes studies of the "slow" physical processes responsible for climate variability on seasonal, interannual, decadal, and centennial timescales to determine its predictability with a particular emphasis on ocean–atmosphere coupling. To do this requires collection and analysis of global observations covering long time periods, lengthening the available data record by assembling comprehensive paleoclimate information, and development of models that couple all the major components of the climate system (atmosphere, ocean, cryosphere, and biosphere). These models can be used for seasonal-to-interannual climate predictions and to project the response of the climate to changes in the abundances of radiatively active gases and aerosols. Comparison of the predictions with the observations will indicate whether human activities are changing the climate in noticeable ways. Thus, continuation of ISCCP is necessary to provide the detailed and long-term observations of cloud variations (and their role in modulating the radiation and hydrological budgets) that are key to studying the coupling of the atmosphere, land surface, cryosphere, and oceans, especially on longer timescales.

One indication of when to stop a project like ISCCP is when it can be replaced by a better observing system. ISCCP currently uses only two wavelengths, so that the obtainable cloud information does not include 1) cloud-base location and layer thickness; 2) particle size, shape, and phase; and 3) the vertical distribution of water, its phase, and particle size distributions within multiple-layered cloud systems. Moreover, the characterization of the diurnal variations of cloud microphysics for upper-level clouds and of the annual cycle of cloud microphysics in the polar regions is incomplete. Some of these problems will yield, in part, to extended and combined analyses of coincident multispectral imager, infrared, and microwave sounder observations already available. Such analyses will also be improved with advanced instruments flying on new research satellites: Tropical Rainfall Measuring Mission, Earth Observing System (AM1 = Terra and PM1), ENVISAT, and the Advanced Earth Observing Satellite-II. However, none of these new missions provides both the global coverage and the diurnal time resolution of the constellation of weather satellites used by ISCCP. Thus, the interpretation of these new cloud measurements in terms of both long-term climate variations and short-term cloud dynamical processes will have a firmer foundation by combining them with the higher time resolution ISCCP datasets covering almost two decades.

Planning for the National Polar Orbiting Environmental Satellite System (NPOESS), a joint effort by NOAA, the Department of Defense, NASA, and EUMETSAT, presents an opportunity to improve the systematic monitoring of clouds with similar coverage and time resolution as ISCCP but with measurements at many more wavelengths. The NPOESS system is three polar orbiting satellites with common instrumentation that will provide global coverage with adequate diurnal (4 h) resolution. Having a set of common instruments would significantly reduce the intercalibration problem and would provide significant improvements in cloud retrievals over ISCCP through the combined analysis of data from an advanced multichannel (at least seven) visible/infrared imager, a microwave imager, infrared and microwave temperature–humidity sounders, and an ozone-measuring instrument. Thus, ISCCP might continue until NPOESS can take over the long-term monitoring of global cloudiness (2009 at the earliest). In the meantime, significant effort should be focused on satellite experiments that provide missing elements of cloud dynamical processes, such as determinations of cloud vertical structure and geostationary observations of cloud system evolution at very high time resolutions (~ 15–30 min).

Acknowledgments. ISCCP has involved efforts by a large number of people. The WCRP director for most of the time was Pierre Morel and is now Harmut Grassl; science advice came from both the International Radiation Commission, represented by Ehrhard Raschke, and the WCRP, represented by T. H. Vonder Haar and now by G. L. Stephens. Participating institutions are the European Space Agency, EUMETSAT, the Japanese Meteorological Agency, Atmospheric Environment Service

(Canada), Colorado State University, University of Wisconsin, National Oceanic and Atmospheric Administration, Centre Meteorologie Service (France), and the National Aeronautics and Space Administration. We are also indebted to the work and advice of many other researchers, but thank particularly G. Seze, P. Minnis, B. A. Wielicki, C. Stubenrauch, D. P. Wylie, Q. Han, G. Tselioudis, B. Lin, and J. Wang. Radiative transfer model and retrieval developments were based on the work of A. A. Lacis, Q. Ma, M. I. Mishchenko, P. Minnis, K.-N. Liou, Q. Han, and Y. Zhang. Over the years we have benefitted from scientific discussions with G. L. Stephens, A. D. Del Genio, J. A. Curry, B. E. Carlson, A. A. Lacis, and B. Cairns. Staff at NASA/GISS that helped make the transition to the new data products are D. E. Beuschel, C. L. Brest, D. Cordero, L. C. Garder, R. Karow, A. Lien, C. Pearl, M. D. Roiter, and M. Rothstein; but most especially A. W. Walker who kept us organized. Statistics and plots were compiled by D. Cordero and graphics done by L. Del Valle.

References

Barker, H. W., 1996: A parameterization for computing grid-averaged solar fluxes for inhomogeneous marine boundary layer clouds. Part I: Methodology and homogeneous biases. *J. Atmos. Sci.,* **53,** 2289–2303.

——, and B. A. Wielicki, 1997: Parameterizing grid-averaged longwave fluxes for inhomogeneous marine boundary layer clouds. *J. Atmos. Sci.,* **54,** 2785–2798.

——, T. J. Curtis, E. Leontyeva, and K. Stamnes, 1998: Optical depth of overcast cloud across Canada: Estimates based on surface pyranometer and satellite measurements. *J. Climate,* **11,** 2980–2994.

Bates, J. J., X. Wu, and D. L. Jackson, 1996: Interannual variability of upper-tropospheric water vapor band brightness temperature. *J. Climate,* **9,** 427–438.

Bishop, J. K. B., W. B. Rossow, and E. G. Dutton, 1997: Surface solar irradiance from the International Satellite Cloud Climatology Project 1983–1991. *J. Geophys. Res.,* **102,** 6883–6910.

Brest, C. L., and W. B. Rossow, 1992: Radiometric calibration and monitoring of NOAA AVHRR data for ISCCP. *Int. J. Remote Sens.,* **13,** 235–273.

——, ——, and M. D. Roiter, 1997: Update of radiance calibrations for ISCCP. *J. Atmos. Oceanic Technol.,* **14,** 1091–1109.

Browning, K. A., 1993: The GEWEX Cloud System Study (GCSS). *Bull. Amer. Meteor. Soc.,* **74,** 387–399.

Cahalan, R. F., W. Ridgway, W. J. Wiscombe, T. L. Bell, and J. B. Snider, 1994a: The albedo of fractal stratocumulus clouds. *J. Atmos. Sci.,* **51,** 2434–2455.

——, ——, ——, S. Gollmer, and Harshvardhan, 1994b: Independent pixel and Monte Carlo estimates of stratocumulus albedo. *J. Atmos. Sci.,* **51,** 3776–3790.

Cairns, B., 1995: Diurnal variations of cloud from ISCCP data. *Atmos. Res.,* **37,** 133–146.

——, A. A. Lacis, and B. E. Carlson, 1999: Absorption within inhomogeneous clouds and its parameterization in general circulation models. *J. Atmos. Sci.,* in press.

Chambers, L. H., B. A. Wielicki, and K. F. Evans, 1997a: Accuracy of the independent pixel approximation for satellite estimates of oceanic boundary layer cloud optical depth. *J. Geophys. Res.,* **102,** 1779–1794.

——, ——, and ——, 1997b: Independent pixel and two-dimensional estimates of Landsat-derived cloud field albedo. *J. Atmos. Sci.,* **54,** 1525–1532.

Chen, S., and R. A. Houze, 1997: Diurnal variation and life-cycle of deep convective systems over the tropical Pacific warm pool. *Quart. J. Roy. Meteor. Soc.,* **123,** 357–388.

——, ——, and B. E. Mapes, 1996: Multiscale variability of deep convection in relation to large-scale circulation in TOGA COARE. *J. Atmos. Sci.,* **53,** 1380–1409.

Chen, T., W. B. Rossow, and Y.-C. Zhang, 1999: Radiative effects of cloud type variations. *J. Climate,* in press.

Coakley, J. A., and F. P. Bretherton, 1982: Cloud cover from high-resolution scanner data: Detecting and allowing for partially filled fields of view. *J. Geophys. Res.,* **87,** 4917–4932.

Curry, J. A., and E. E. Ebert, 1992: Annual cycle of radiation fluxes over the Arctic Ocean: Sensitivity to cloud optical properties. *J. Climate,* **5,** 1267–1280.

——, W. B. Rossow, D. Randall, and J. L. Schramm, 1996: Overview of Arctic cloud and radiation characteristics. *J. Climate,* **9,** 1731–1764.

Davis, A., A. Marshak, R. Cahalan, and W. Wiscombe, 1997: The Landsat scale break in stratocumulus as a three-dimensional radiative transfer effect: Implications for cloud remote sensing. *J. Atmos. Sci.,* **54,** 241–260.

Descloitres, J. C., J. C. Buriez, F. Parol, and Y. Fouquart, 1998: POLDER observations of cloud bidirectional reflectances compared to a plane-parallel model using the International Satellite Cloud Climatology Project cloud phase functions. *J. Geophys. Res.,* **103,** 11 411–11 418.

Desormeaux, Y., W. B. Rossow, C. L. Brest, and G. G. Campbell, 1993: Normalization and calibration of geostationary satellite radiances for ISCCP. *J. Atmos. Oceanic Technol.,* **10,** 304–325.

Di Girolamo, L., and R. Davies, 1997: Cloud fraction errors caused by finite resolution measurements. *J. Geophys. Res.,* **102,** 1739–1756.

Doutriaux-Boucher, M., and G. Seze, 1998: Significant changes between the ISCCP C and D cloud climatologies. *Geophys. Res. Lett.,* **25,** 4193–4196.

Feigelson, E. M., 1984: *Radiation in a Cloudy Atmosphere.* D. Reidel, 293 pp.

Foot, J. S., 1988: Some observations of the optical properties of clouds. II. Cirrus. *Quart. J. Roy. Meteor. Soc.,* **114,** 145–164.

Francis, P. N., 1995: Some aircraft observations of the scattering properties of ice crystals. *J. Atmos. Sci.,* **52,** 1142–1154.

Hahn, C. J., S. G. Warren, and J. London, 1995: The effect of moonlight on observation of cloud cover at night, and application to cloud climatology. *J. Climate,* **8,** 1429–1446.

Han, Q.-Y., W. B. Rossow, and A. A. Lacis, 1994: Near-global survey of effective cloud droplet radii in liquid water clouds using ISCCP data. *J. Climate,* **7,** 465–497.

——, R. Welch, A. White, and J. Chou, 1995: Validation of satellite retrievals of cloud microphysics and liquid water path using observations from FIRE. *J. Atmos. Sci.,* **52,** 4183–4195.

——, ——, J. Chou, K.-S. Kuo, and R. M. Welch, 1999: The effects of aspect ratio and surface roughness on satellite retrievals of ice-cloud properties. *J. Quart. Spectrosc. Radiat. Trans.,* **63,** 559–583.

Hansen, J. E., and L. D. Travis, 1974: Light scattering in planetary atmospheres. *Space Sci. Rev.,* **16,** 527–610.

Heymsfield, A. J., 1972: Ice crystal terminal velocities. *J. Atmos. Sci.*, **29,** 1348–1357.

Hobbs, P. V., 1974: *Ice Physics.* Clarendon, 837 pp.

Iaquinta, J., H. Isaka, and P. Personne, 1995: Scattering phase function of bullet rosette ice crystals. *J. Atmos. Sci.*, **52,** 1401–1413.

Jin, Y., and W. B. Rossow, 1997: Detection of cirrus overlapping low-level clouds. *J. Geophys. Res.*, **102,** 1727–1737.

——, ——, and D. P. Wylie, 1996: Comparison of the climatologies of high-level clouds from HIRS and ISCCP. *J. Climate*, **9,** 2850–2879.

Key, J., and R. G. Barry, 1989: Cloud cover analysis with Arctic AVHRR data. 1. Cloud detection. *J. Geophys. Res.*, **94,** 8521–8535.

Klein, S. A., and D. L. Hartmann, 1993: Spurious trend in the ISCCP C2 dataset. *Geophys. Res. Lett.*, **20,** 455–458.

——, and C. Jacob, 1999: Validation and sensitivities of frontal clouds simulated by the ECMWF model. *Mon. Wea. Rev.*, **127,** 2514–2531.

Kobayashi, T., 1993: Effects due to cloud geometry on biases in the albedo derived from radiance measurements. *J. Climate*, **6,** 120–128.

Kondragunta, C. R., and A. Gruber, 1994: Diurnal variations of the ISCCP cloudiness. *Geophys. Res. Lett.*, **21,** 2015–2018.

Laing, A. G., and M. Fritsch, 1993a: Mesoscale convective complexes in Africa. *Mon. Wea. Rev.*, **121,** 2254–2263.

——, and ——, 1993b: Mesoscale convective complexes over the Indian monsoon region. *J. Climate*, **6,** 911–919.

Lau, N.-C., and M. W. Crane, 1995: A satellite view of the synoptic-scale organization of cloud properties in midlatitude and tropical circulation systems. *Mon. Wea. Rev.*, **123,** 1984–2006.

Leontyeva, E., and K. Stamnes, 1994: Estimation of cloud optical thickness from ground-based measurements of incoming solar radiation in the Arctic. *J. Climate*, **7,** 566–578.

Liao, X., W. B. Rossow, and D. Rind, 1995a: Comparison between SAGE II and ISCCP high-level clouds, Part I: Global and zonal mean cloud amounts. *J. Geophys. Res.*, **100,** 1121–1135.

——, ——, and ——, 1995b: Comparison between SAGE II and ISCCP high-level clouds, Part II: Locating cloud tops. *J. Geophys. Res.*, **100,** 1137–1147.

Lin, B., and W. B. Rossow, 1994: Observations of cloud liquid water path over oceans: Optical and microwave remote sensing methods. *J. Geophys. Res.*, **99,** 20 907–20 927.

——, and ——, 1996: Seasonal variation of liquid and ice water path in nonprecipitating clouds over oceans. *J. Climate*, **9,** 2890–2902.

——, and ——, 1997: Precipitation water path and rainfall rate estimates for oceans using special sensor microwave imager and International Satellite Cloud Climatology Project data. *J. Geophys. Res.*, **102,** 9359–9374.

——, B. A. Wielicki, P. Minnis, and W. B. Rossow, 1998a: Estimation of water cloud properties from satellite microwave, infrared and visible measurements in oceanic environments. 1. Microwave brightness temperature simulations. *J. Geophys. Res.*, **103,** 3873–3886.

——, P. Minnis, B. Wielicki, D. R. Doelling, R. Palikonda, D. F. Young, and T. Uttal, 1998b: Estimation of water cloud properties from satellite microwave, infrared and visible measurements in oceanic environments. 2. Results. *J. Geophys. Res.*, **103,** 3887–3905.

Liu, G., J. A. Curry, and R.-S. Sheu, 1995: Classification of clouds over the western equatorial Pacific Ocean using combined infrared and microwave satellite data. *J. Geophys. Res.*, **100,** 13 811–13 826.

Loeb, N. G., and J. A. Coakley, 1998: Inference of marine stratus cloud optical depths from satellite measurements: Does 1D theory apply? *J. Climate*, **11,** 215–233.

Lubin, D., and D. A. Harper, 1996: Cloud radiative properties over the South Pole from AVHRR infrared data. *J. Climate*, **9,** 3405–3418.

Machado, L. A. T., and W. B. Rossow, 1993: Structural characteristics and radiative properties of tropical cloud clusters. *Mon. Wea. Rev.*, **121,** 3234–3260.

——, ——, R. L. Guedes, and A. W. Walker, 1998: Life cycle variations of mesoscale convective systems over the Americas. *Mon. Wea. Rev.*, **126,** 1630–1654.

Macke, A., 1993: Scattering of light by polyhedral ice crystals. *Appl. Opt.*, **32,** 2780–2788.

——, J. Mueller, and E. Raschke, 1996: Single scattering properties of atmospheric ice crystals. *J. Atmos. Sci.*, **53,** 2813–2825.

Mapes, B. E., 1993: Gregarious tropical convection. *J. Atmos. Sci.*, **50,** 2026–2037.

Marshak, A., A. Davis, W. Wiscombe, and R. Cahalan, 1995: Radiative smoothing in fractal clouds. *J. Geophys. Res.*, **100,** 26 247–26 261.

——, ——, ——, W. Ridgway, and R. Cahalan, 1998: Biases in shortwave column absorption in the presence of fractal clouds. *J. Climate*, **11,** 431–446.

Minnis, P., 1989: Viewing zenith angle dependence of cloudiness determined from coincident GOES EAST and GOES WEST data. *J. Geophys. Res.*, **94,** 2303–2320.

——, D. F. Young, C. W. Fairall, and J. B. Snider, 1992: Stratocumulus cloud properties from simultaneous satellite and island-based instrumentation during FIRE. *J. Appl. Meteor.*, **31,** 317–339.

——, P. W. Heck, and D. F. Young, 1993a: Inference of cirrus cloud properties using satellite-observed visible and infrared radiances. Part II: Verification of theoretical cirrus radiative properties. *J. Atmos. Sci.*, **50,** 1305–1322.

——, K.-N. Liou, and Y. Takano, 1993b: Inference of cirrus cloud properties using satellite-observed visible and infrared radiances. Part I: Parameterization of radiance fields. *J. Atmos. Sci.*, **50,** 1279–1304.

Mishchenko, M. I., W. B. Rossow, A. Macke, and A. A. Lacis, 1996: Sensitivity of cirrus cloud albedo, bidirectional reflectance, and optical thickness retrieval accuracy to ice-particle shape. *J. Geophys. Res.*, **101,** 16 973–16 985.

Mokhov, I. I., and M. E. Schlesinger, 1993: Analysis of global cloudiness, 1, Comparison of ISCCP, Meteor and Nimbus 7 satellite data. *J. Geophys. Res.*, **98,** 12 849–12 868.

——, and ——, 1994: Analysis of global cloudiness, 2, Comparison of ground-based and satellite-based cloud climatologies. *J. Geophys. Res.*, **99,** 17 045–17 065.

Muinonen, K., K. Lumme, J. Peltoniemi, and W. M. Irvine, 1989: Light scattering by randomly oriented crystals. *Appl. Opt.*, **28,** 3051–3060.

Nakajima, T., and M. D. King, 1990: Determination of the optical thickness and effective particle radius of clouds from reflected solar radiation measurements. Part I: Theory. *J. Atmos. Sci.*, **47,** 1878–1893.

Peixoto, J. P., and A. H. Oort, 1992: *Physics of Climate.* American Institute of Physics, 520 pp.

Randall, D. A., B. Albrecht, S. Cox, D. Johnson, P. Minnis, W. Rossow, and D. O'C. Starr, 1996: On FIRE at ten. *Advances in Geophysics,* Vol. 38, Academic Press, 37–177.

Raschke, E., J. Schmetz, J. Heintzenberg, R. Kandel, and R. Saunders, 1990: The International Cirrus Experiment (ICE)—A joint European effort. *Eur. Space Agency J.,* **14,** 193–199.

——, P. Bauer, and H. J. Lutz, 1992: Remote sensing of clouds and surface radiation budget over polar regions. *Int. J. Remote Sens.,* **13,** 13–22.

——, P. Flamont, Y. Fouquart, P. Hignett, H. Isaka, P. Jonas, and H. Sundqvist, 1998: Cloud-radiation studies during the European Cloud and Radiation Experiment (EUCREX). *Surv. Geophys.,* in press.

Ricchiazzi, P., C. Gautier, and D. Lubin, 1995: Cloud scattering optical depth and local surface albedo in the Antarctic: Simultaneous retrieval using ground-based radiometry. *J. Geophys. Res.,* **100,** 21 091–21 104.

Rossow, W. B., Ed., 1981: Clouds in climate: Modeling and satellite observational studies. Rep. of workshop held at Goddard Institute for Space Studies, October 1980, New York, NY 222 pp. [Available from NASA Goddard Institute for Space Studies, 2880 Broadway, New York, NY 10025.]

——, 1989: Measuring cloud properties from space: A review. *J. Climate,* **2,** 201–213.

——, and R. A. Schiffer, 1991: ISCCP cloud data products. *Bull. Amer. Meteor. Soc.,* **72,** 2–20.

——, and L. C. Garder, 1993a: Cloud detection using satellite measurements of infrared and visible radiances for ISCCP. *J. Climate,* **6,** 2341–2369.

——, and ——, 1993b: Validation of ISCCP cloud detections. *J. Climate,* **6,** 2370–2393.

——, and B. Cairns, 1995: Monitoring changes of clouds. *Climate Change,* **31,** 305–347.

——, and Y.-C. Zhang, 1995: Calculation of surface and top-of-atmosphere radiative fluxes from physical quantities based on ISCCP datasets, Part II: Validation and first results. *J. Geophys. Res.,* **100,** 1167–1197.

——, and Coauthors, 1985: ISCCP cloud algorithm intercomparison. *J. Climate Appl. Meteor.,* **24,** 877–903.

——, E. Kinsella, A. Wolf, and L. Garder, 1987: International Satellite Cloud Climatology Project (ISCCP) description of reduced resolution radiance data. WMO/TD 58 (revised), World Climate Research Programme (ICSU and WMO), 143 pp.

——, L. C. Garder, and A. A. Lacis, 1989: Global, seasonal cloud variations from satellite radiance measurements. Part I: Sensitivity of analysis. *J. Climate,* **2,** 419–462.

——, ——, P.-J. Lu, and A. Walker, 1991: International Satellite Cloud Climatology Project (ISCCP) documentation of cloud data. WMO/TD 266 (revised), World Climate Research Programme (ICSU and WMO), 76 pp plus three appendices.

——, Y. Desormeaux, C. L. Brest, and A. Walker, 1992: International Satellite Cloud Climatology Project (ISCCP) radiance calibration report. WMO/TD 520, World Climate Research Programme (ICSU and WMO), 104 pp.

——, A. W. Walker, and L. C. Garder, 1993: Comparison of ISCCP and other cloud amounts. *J. Climate,* **6,** 2394–2418.

——, C. L. Brest, and M. Roiter, 1996a: International Satellite Cloud Climatology Project (ISCCP) new radiance calibrations. WMO/TD 736, World Climate Research Programme (ICSU and WMO), 76 pp.

——, M. D. Roiter, and C. L. Brest, 1996b: International Satellite Cloud Climatology Project (ISCCP) updated description of reduced resolution radiance data. WMO/TD 58 (revised), World Climate Research Programme (ICSU and WMO), 163 pp.

——, A. W. Walker, D. Beuschel, and M. Roiter, 1996c: International Satellite Cloud Climatology Project (ISCCP) description of new cloud datasets. WMO/TD 737, World Climate Research Programme (ICSU and WMO), 115 pp.

Rozendaal, M. A., C. B. Leovy, and S. A. Klein, 1995: An observational study of diurnal variations of marine stratiform cloud. *J. Climate,* **8,** 1795–1809.

Sassen, K., and B. S. Cho, 1992: Subvisual-thin cirrus lidar dataset for satellite verification and climatological research. *J. Appl. Meteor.,* **31,** 1275–1285.

Schiffer, R. A., and W. B. Rossow, 1983: The International Satellite Cloud Climatology Project (ISCCP): The first project of the World Climate Research Programme. *Bull. Amer. Meteor. Soc.,* **64,** 779–784.

——, and ——, 1985: ISCCP global radiance data set: A new resource for climate research. *Bull. Amer. Meteor. Soc.,* **66,** 1498–1505.

Schweiger, J. A., and J. R. Key, 1992: Arctic cloudiness: Comparison of ISCCP-C2 and Nimbus-7 satellite-derived cloud products with a surface-based cloud climatology. *J. Climate,* **5,** 1514–1527.

Sheu, R.-S., J. A. Curry, and G. Liu, 1997: Vertical stratification of tropical cloud properties as determined from satellites. *J. Geophys. Res.,* **102,** 4231–4245.

Song, N., D. O'C. Starr, D. J. Wuebbles, A. Williams, and S. M. Larson, 1996: Volcanic aerosols and interannual variation of high clouds. *Geophys. Res. Lett.,* **23,** 2657–2660.

Spinhirne, J. D., W. D. Hart, and D. L. Hlavka, 1996: Cirrus infrared parameters and shortwave reflectance relations from observations. *J. Atmos. Sci.,* **53,** 1438–1458.

Stone, R. S., 1993: Properties of austral winter clouds derived from radiometric profiles at the South Pole. *J. Geophys. Res.,* **98,** 12 961–12 971.

Stubenrauch, C. J., W. B. Rossow, F. Cheruy, A. Chedin, and N. A. Scott, 1999a: Clouds as seen by satellite sounders (3I) and imagers (ISCCP). Part I: Evaluation of cloud parameters. *J. Climate,* **12,** 2189–2213.

——, ——, N. A. Scott, and A. Chedin, 1999b: Clouds as seen by satellite sounders (3I) and imagers (ISCCP). Part III: Combining 3I and ISCCP cloud parameters for better understanding of cloud radiative effects. *J. Climate,* in press.

Sun, Z., and K. P. Shine, 1995: Parameterization of ice cloud radiative properties and its application to the potential climatic importance of mixed-phase clouds. *J. Climate,* **8,** 1874–1888.

Takano, Y., and K.-N. Liou, 1989: Solar radiative transfer in cirrus clouds. Part I: Single scattering and optical properties of hexagonal ice crystals. *J. Atmos. Sci.,* **46,** 3–19.

Tian, L., and J. Curry, 1989: Cloud overlap statistics. *J. Geophys. Res.,* **94,** 9925–9935.

Tselioudis, G., W. B. Rossow, and D. Rind, 1992: Global patterns of cloud optical thickness variation with temperature. *J. Climate,* **5,** 1484–1495.

——, Y.-C. Zhang, and W. B. Rossow, 1999: Cloud and radiation variations associated with northern midlatitude low and high sea level pressure regimes. *J. Climate*, in press.

Wang, J., 1997: Determination of cloud vertical structure from upper air observations and its effects on atmospheric circulation in a GCM. Ph.D. dissertation, Columbia University, 233 pp.

——, and W. B. Rossow, 1995: Determination of cloud vertical structure from upper air observations. *J. Appl. Meteor.*, **34,** 2243–2258.

——, ——, T. Uttal, and M. Rozendaal, 1999: Variability of cloud vertical structure during ASTEX from a combination of rawinsonde, radar, ceilometer and satellite data. *Mon. Wea. Rev.*, **127,** 2484–2502.

Warren, S. G., C. J. Hahn, J. London, R. M. Chervin, and R. L. Jenne, 1986: Global distribution of total cloud and cloud type amounts over land. NCAR Tech. Note TN-273 and STR/DOE Tech. Rep. ER/60085-HI, 29 pp. plus 200 maps. [NTIS DE87-00-6903.]

——, ——, ——, ——, and ——, 1988: Global distribution of total cloud and cloud type amounts over the ocean. NCAR Tech. Note TN-317 and STR/DOE Tech. Rep. ER-0406, 42 pp. plus 170 maps. [NTIS DE90-00-3187.]

Wielicki, B. A., and L. Parker, 1992: On the determination of cloud cover from satellite sensors: The effect of sensor spatial resolution. *J. Geophys. Res.*, **97,** 12 799–12 823.

Wylie, D. P., and P. H. Wang, 1997: Comparison of cloud frequency data from the high-resolution infrared radiometer sounder and the Stratospheric Aerosol and Gas Experiment II. *J. Geophys. Res.*, **102,** 29 893–29 900.

——, W. P. Menzel, H. M. Woolf, and K. I. Strabala, 1994: Four years of global cirrus cloud statistics using HIRS. *J. Climate*, **7,** 1972–1986.

Yamanouchi, T., and S. Kawaguchi, 1992: Cloud distribution in the Antarctic from AVHRR data and radiation measurements at the surface. *Int. J. Remote Sens.*, **13,** 111–127.

Zhang, Y.-C., W. B. Rossow, and A. A. Lacis, 1995: Circulation of surface and top-of-atmosphere radiative fluxes from physical quantities based on ISCCP datasets, Part I: Method and sensitivity to input data uncertainties. *J. Geophys. Res.*, **100,** 1149–1165.